Published in final edited form as:
*Neuroimage*. 2011 June 15; 56(4): 2183–2199. doi:10.1016/j.neuroimage.2011.03.041.

# Not one extrastriate body area: Using anatomical landmarks, hMT+, and visual field maps to parcellate limb-selective activations in human lateral occipitotemporal cortex

**Kevin S. Weiner**[1] and **Kalanit Grill-Spector**[1,2]

[1] Department of Psychology, Stanford University, Stanford, CA 94305

[2] Neuroscience Institute, Stanford University, Stanford, CA 94305

## Abstract

The prevailing view of human lateral occipitotemporal cortex (LOTC) organization suggests a single area selective for images of the human body (extrastriate body area, EBA) that highly overlaps with the human motion-selective complex (hMT+). Using functional magnetic resonance imaging with higher resolution (1.5mm voxels) than past studies (3–4mm voxels), we examined the fine-scale spatial organization of these activations relative to each other, as well as to visual field maps in LOTC. Rather than one contiguous EBA highly overlapping hMT+, results indicate three limb-selective activations organized in a crescent surrounding hMT+: (1) an activation posterior to hMT+ on the lateral occipital sulcus/middle occipital gyrus (LOS/MOG) overlapping the lower vertical meridian shared between visual field maps LO-2 and TO-1, (2) an activation anterior to hMT+ on the middle temporal gyrus (MTG) consistently overlapping the lower vertical meridian of TO-2 and extending outside presently defined visual field maps, and (3) an activation inferior to hMT+ on the inferotemporal gyrus (ITG) overlapping the parafoveal representation of the TO cluster. This crescent organization of limb-selective activations surrounding hMT+ is reproducible over a span of three years and is consistent across different image types used for localization. Further, these regions exhibit differential position properties: preference for contralateral image presentation decreases and preference for foveal presentation increases from the limb-selective LOS to the MTG. Finally, the relationship between limb-selective activations and visual field maps extends to the dorsal stream where a posterior IPS activation overlaps V7. Overall, our measurements demonstrate a series of LOTC limb-selective activations that 1) have separate anatomical and functional boundaries, 2) overlap distinct visual field maps, and 3) illustrate differential position properties. These findings indicate that category selectivity alone is an insufficient organization principle for defining brain areas. Instead, multiple properties are necessary in order to parcellate and understand the functional organization of high-level visual cortex.

### Keywords

fMRI; extrastriate body area; object recognition; visual field maps; human area MT

Corresponding Author: Kevin S. Weiner, Department of Psychology, Stanford University, Stanford, California, 94305, kweiner@stanford.edu.

## INTRODUCTION

Neuroimaging studies in the field of high level vision have identified an activation in human lateral occipitotemporal cortex (LOTC) known as the extrastriate body area (EBA) that is selective for images of the body and body parts relative to a variety of control images (Downing et al., 2001; Orlov et al., 2010; Peelen and Downing, 2007; Pinsk et al., 2009; Schwarzlose et al., 2008; Spiridon et al., 2006). Though this activation is typically localized by contrasting neural responses to images of headless bodies and body parts (most often limbs, such as arms and legs), relative to objects, faces, and places, there is considerable variability in the types of images and statistical contrasts used to localize the EBA (Supplemental Table 1). Additionally, there is a lack of anatomical and functional specificity in the boundaries demarcating the EBA. Researchers loosely identify the EBA as a large swath of cortex extending from the lateral occipital sulcus (LOS) to portions of the inferotemporal gyrus (ITG), often encompassing the ascending limb of the posterior inferotemporal sulcus (pITS; Peelen and Downing, 2007; Peelen et al., 2006). However, the pITS is also the location of an extensively studied region involved in motion perception, the human MT+ complex (hMT+; DeYoe et al., 1996; Dumoulin et al., 2000; Huk et al., 2002; Tootell et al., 1995). Even though the EBA and hMT+ are accepted to be cortical neighbors on the pITS (Downing et al., 2007), no group has examined their spatial relationship with high-resolution fMRI, leaving open the question: *What is the fine-scale spatial organization among body part- and motion-selective voxels in LOTC?*

The prevailing view in the field is that the EBA is a distinct visual area based on its body part selectivity (Downing et al., 2001; Kanwisher, 2010; Op de Beeck et al., 2008; Peelen and Downing, 2007) and that it substantially overlaps hMT+ on the pITS (Downing et al., 2007; Peelen and Downing, 2007). This suggests an organization where these two regions share a large extent of cortex with the EBA located posterior to and overlapping with hMT+ (Figure 1a; based on descriptions by Peelen and Downing, 2007; Peelen et al., 2006). However, when using un-segmented brain volume visualizations, it is complicated to get an accurate understanding of the spatial relationship between these LOTC activations because the apparent organization is dependent on the view axis. For example, in Figure 2 of Downing et al., 2007, the EBA appears to be posterior and superior to hMT+ on the sagittal view, but on the axial view, the EBA extends anterior to hMT+ onto the middle temporal gyrus (MTG). Indeed, with improved visualizations on the inflated cortical surface rather than on the un-segmented brain volume, the EBA does not appear as a single spherical activation posterior to hMT+ (see Figures 2 and 3 from Spiridon et al., 2006; Supplemental Figure 3 from Schwarzlose et al., 2008). Instead, the EBA seems to surround hMT+. A common feature we infer from these cortical surface visualizations is an organization containing body part-selective voxels in a ring-like structure sparing a central, non-overlapping portion of hMT+ (Figure 1b). Though this ring structure has been illustrated also in EBA studies that have not included hMT+ (Figure 6 from Pinsk et al., 2009; Figure 2 from Orlov et al., 2010), this ring organization has never been referenced or examined in prior studies.

While at first glance, it may not seem crucial if the EBA is arranged either as a spherical cluster or a ring (as long as it contiguous), a contiguous activation does not indicate homogeneity at either the voxel or neural level. An analogous ring organization exists in early visual cortex where eccentricity bands span a contiguous set of voxels surrounding the confluent fovea. However, researchers do not average data across an entire eccentricity band because it is well known that receptive field properties across an eccentricity band differ across adjacent visual areas and their properties become more differentiated as the cortical distance between areas increases (Boussaoud et al., 1991; Dumoulin and Wandell, 2008; Grill-Spector and Malach, 2004). Thus, in fMRI studies, continuous eccentricity bands are

divided into distinct visual areas using a separate polar angle measurement. Consequently, even if the EBA is observed as a continuous ring of activation, it raises two questions*: (1) Is the EBA a homogeneous cortical region, or does it include separate heterogeneous activations? (2) What criteria should be used to divide this activation?*

Classic neuroscience studies use several independent criteria to guide the decision of parcellating cortical regions into distinct areas (Desimone and Ungerleider, 1986; Felleman and Van Essen, 1991 are two such examples). These criteria include anatomical location, cytoarchitecture, connectivity, topographic organization, and function. Though we cannot use all of these criteria when noninvasively measuring functional activations in humans with fMRI, we can directly measure anatomical location, topographic organization, and function, as well as use knowledge from prior studies examining cytoarchitecture and connectivity to support or refute further parcellation.

One way to apply these methods to the current research is to examine the relation between body part-selective activations and the region they neighbor: hMT+. In humans, hMT+ is identified based on its motion selectivity and location in the pITS (Dumoulin et al., 2000). Examining the relation between the body part-selective activations and hMT+ is particularly appealing because the posterior component of the hMT+ complex, area MT (also referred to as V5; Watson et al., 1993; Zeki et al., 1991), is one of only a handful of brain areas widely accepted to exist across primates (Kaas, 2005; Zeki, 2004). Anatomical studies of postmortem human brains indicate that area MT is a distinct ovoid region that is densely myelinated. The cortex surrounding MT is crescent-shaped, has a different cytoarchitecture, is less myelinated, and understood to be a region separate from MT known as MT crescent (MTc; Tootell and Taylor, 1995). Moreover, anatomical studies in both old and new world monkeys document a similar MTc region that is distinct from MT (owl monkeys: Kaas and Morel, 1993; Tootell et al., 1985; green monkeys and macaques: Tootell and Taylor, 1995). In macaques, MTc has been further separated into areas V4t and FST based on differences in motion and position sensitivity, as well as cortico-cortical connections (Desimone and Ungerleider, 1986; Felleman and Van Essen, 1991). Thus, in both humans and monkeys, the underlying cytoarchitecture within MT is different than its immediate surround, where MTc has been identified as a single area by some researchers or several distinct areas by others. This divided crescent suggests a third possible organization of LOTC (Figure 1c) where several limb-selective activations surround hMT+ based on their anatomical location and potential underlying differences in cytoarchitecture and function.

Another source of information for deciding whether to split or to combine functional activations in visual cortex is the finding that visual field maps consistently co-localize with specific anatomical landmarks. MT, for example, contains a hemifield map starting from the lower vertical meridian in the pITS ending with the upper vertical meridian more anteriorly. Eccentricity is organized such that the foveal representation is located on the inferior portion of the pITS and the peripheral representation extends to the superior portion of the pITS (Huk et al., 2002). This relationship between anatomical location and visual field maps is prevalent in early visual cortex and throughout LOTC (Wandell et al., 2007). It is possible that the body part-selective activations potentially surrounding hMT+ (1) can be reliably dissociated based on anatomical location and (2) that this parcellation can be verified by visual field maps. Further, improved imaging of LOTC with high-resolution fMRI will reduce partial voluming effects, address overlap effects, and aid in defining this portion of cortex more accurately. We recently used these methods in ventral temporal cortex, discovering a consistent topography of face- and limb-selective activations both relative to each other as well as to known visual field maps on the fusiform gyrus and occipitotemporal sulcus (Weiner and Grill-Spector, 2010).

In the present study, we examined the spatial organization of the EBA relative to hMT+ and known LOTC visual field maps at a finer spatial scale in order to address the following questions:

1. Are there separate limb-selective components with distinct anatomical locations surrounding hMT+ (Figure 1)?
2. Does the location of LOTC visual field maps support or refute the parcellation of limb-selective activations based on anatomical location?
3. If LOTC limb-selective activations can be reliably parcellated, can they be functionally dissociated based on their category selectivity and position sensitivity?

## MATERIALS AND METHODS

### Subjects

Nine subjects (3 female, ages 24–39) participated in three experiments: six category experiment (sessions one and two), motion experiment (sessions one and two), and visual field mapping (session three). Six of these subjects also participated in an experiment during which we measured responses to limbs across three positions in the visual field (session four). A subset of these subjects also participated in additional sessions of control mapping experiments used to parcellate hMT+ into MT and MST, and to examine the effect of larger voxels and different types of body images on the resulting LOTC maps. All subjects participated in scans during which we acquired a whole brain anatomical volume. Written consent was obtained from each subject. Procedures were approved by the Stanford Internal Review Board on human subjects research.

### Experimental Procedures

**Six category experiment—**Subjects participated in 2–3 runs of this experiment during which they viewed images of faces, limbs, flowers, cars, guitars, houses, and scrambled versions of these exemplars in 12-s blocks (Figure 2a). Each image was presented for 750-ms followed by a 250-ms blank. Faces, flowers, houses, cars, and guitars were from a database used in our previous studies (Grill-Spector and Kanwisher, 2005; Grill-Spector et al., 2004; Sayres and Grill-Spector, 2008; Weiner and Grill-Spector, 2010; Weiner et al., 2010). Limb stimuli included both upper and lower limbs, always included the digits, and sometimes included pairs of arms and legs and were used in recently published studies from our lab (Sayres and Grill-Spector, 2008; Weiner and Grill-Spector, 2010; Weiner et al., 2010). We used images of limbs because they are the most common type of body part images used to localize the EBA and arms/legs are included in images of headless bodies (Supplemental Table 1). We used gray level images subtending a visual angle of 7.125º centered on the fovea presented with Psychophysics Toolbox (Brainard, 1997) using code written in MATLAB (The Mathworks, Natick, MA). Exemplars from each of our categories appeared in various viewing angles. Each run consisted of 4 blocks of each condition and 6 blank blocks. Subjects maintained fixation and performed a 1-back task, responding by button press when two consecutive images were identical. Categories were counterbalanced within each run and images were not repeated across runs. Results from this experiment were reported in recent publications examining the functional organization of ventral temporal cortex (Weiner and Grill-Spector, 2010; Weiner et al., 2010). All subjects participated in two sessions of this experiment on different days and resolutions.

To validate that category effects in LOTC are not simply inherited from earlier visual areas or driven by low-level differences across images of various categories, we extracted signals from hV4 (defined by visual field mapping, see below) in each subject. Results of this analysis (Figure 3) across both sessions illustrates that hV4 responds non-selectivity to

images of different categories, as well as to scrambled images. Thus, LOTC results are not simply due to low-level visual differences across images.

**Motion experiment—**Subjects viewed 6 alternations of 16-s blocks of low contrast expanding and contracting concentric gratings and 16-s blocks of identical stationary gratings while fixating (Figure 2b). We defined hMT+ as a region in the posterior inferior temporal sulcus (ITS) that responded more strongly to moving versus stationary gratings ($t > 3$; $p < .002$, voxel-level, uncorrected; Dumoulin et al., 2000; Tootell et al., 1995). All subjects participated in two sessions of this experiment on different days.

**Visual field mapping—**We defined visual field maps using separate retinotopic mapping scans using black and white checkerboard stimuli. During each run, subjects performed a fixation task during which they responded by button press when the fixation point changed color (Figure 2c). Three subjects participated in traditional polar angle scans using a rotating checkerboard wedge and eccentricity scans using an expanding checkerboard ring (at least two runs of each; see Sayres and Grill-Spector, 2008). Six subjects participated in 4–8 runs of visual field mapping scans using checkerboard bar stimuli (as in Amano et al., 2009; Dumoulin and Wandell, 2008). The stimuli included bar apertures that swept across the visual field exposing black and white checkerboard contrast patterns. At regular intervals, the apertures were removed and subjects viewed a mean luminance gray background with a fixation. There were four bar orientations (0, 45, 90, and 135° from vertical) with two different motion directions orthogonal to each bar orientation, generating a total of eight different bar configurations within a given run of 240s. These stimuli are effective in measuring visual field maps with large receptive fields in LOTC (Amano et al., 2009; Dumoulin and Wandell, 2008; Winawer et al., 2010).

In all nine subjects (18 hemispheres), we identified visual field maps V1, V2, V3, hV4, V3ab, V7 (also referred to as IPS-0), VO-1, VO-2, LO-1, LO-2, TO-1, and TO-2 (Figure 4). V3ab has been recently divided into two further components V3c and V3d, respectively (Georgieva et al., 2009; Kolster et al., 2010). Because these four components are not crucial for the current study, we label this region as V3ab. Further, an alternative organization has been proposed for hMT+ proposing a series of four (rather than two) maps in hMT+ (MT, MSTv, pV4t, and pFST; Kolster et al., 2010; Pitzalis et al., 2010), but based on the visual field mapping stimuli used for the current study, the TO-1/2 organization is more applicable.

**Three-position experiment—**Six of the nine subjects participated in an experiment in which they viewed images of limbs (both upper and lower), faces, and houses presented in 12-s blocks at fixation or 4° to the right or to the left of fixation. We report the data for limb images only, as they are the ones driving the responses in the regions of interest in the present study. Images subtended 2.5° of visual angle at each position. In each 12-s block, different images of a single category were shown at a one position at a rate of 1Hz. Image blocks were interleaved with baseline blocks (grayscale screen with fixation point) lasting 12-s. Each subject participated in 8–12 runs, where each run contained one block of each position and category. Subjects were instructed to fixate and categorize images within 1.5-s of a prompt, which was provided by the dimming of the fixation cross. The dimming prompt occurred randomly, with a 1.5-s to 3.5-s interval between prompts, and was not synchronized to stimulus onsets. Subjects' responses were recorded via a button box. Before scanning, subjects practiced this task to minimize false alarms. Runs for which overall categorization performance was low (60%) due to a decrease in a subjects' overall vigilance were excluded from fMRI analyses (see Sayres and Grill-Spector, 2008 for details).

**MST localizer—**Visual field maps TO-1 and TO-2 correspond to functional subdivisions of hMT+: MT and MST, respectively (Amano et al., 2009). To relate the spatial

organization of our limb-selective activations to MT and MST defined by their differential motion selectivity, three of our subjects participated in a session of MST localizer scans. These scans contained 6 alternations of 16-s blocks of moving and stationary dots presented either foveally (2 runs), 10° to the right (2 runs), or 10° to the left of fixation (2 runs). MST was defined as those voxels responding to moving vs. stationary dots in the ipsilateral visual field (see Huk et al., 2002 and Amano et al., 2009 for details).

**Control mapping experiments with different body part images—**Three years after scanning the original six category localizer, we were able to bring back three of the original subjects to participate in additional experiments: 1) original six category localizer, 2) six category localizer, but with images of headless bodies instead of limbs and 3) seven category localizer with exemplars of different body parts. By running the original six category localizer, we were able to determine the consistency of the organization of limb-selective voxels in LOTC over a span of three years. By running the two new experiments, we were able to examine the sensitivity of the spatial relationship between LOTC voxels selective for images of bodies and body parts relative to hMT+ when using different exemplars. Each of the three subjects participated in 2 runs of these experiments, where the two new experiments had the same experimental design as the six category localizer with each run consisting of 4 blocks of each condition and 6 blank blocks. Each image was presented for 750-ms followed by a 250-ms blank resulting in 12 exemplars within a 12-s block. Subjects maintained fixation and performed a 1-back task. The first control experiment used the exact face, car, guitar, flower, and house exemplars as in the six category localizer, but instead of limbs, we used images of headless bodies, which were obtained from the Downing lab and have been used in recent studies (Supplemental Table 1; Downing et al., 2007; Bracci et al., 2010; Jastorff et al., 2010). The motivation for this experimental design was twofold: 1) by using identical control images as in the original six category localizer, we varied only one parameter to elucidate how changing the exemplars from limbs to headless bodies affects the resulting LOTC maps and 2) by using the same headless body images as recent studies, subjects viewed typical stimuli used by other groups to localize the EBA. The second control experiment used completely new images displaying different types of body parts (torsos, headless bodies, legs, and hands), as well as different control images (chairs, faces, and houses). Torso, leg, and headless body images were the same as those used in a recent study by Orlov and colleagues (2010), and chair images were the same as those used in recent publications (Downing et al., 2007; Bracci et al., 2010; Jastorff et al., 2010). By using completely different stimuli used to localize body part-selective voxels in LOTC, we were able to examine whether the crescent organization surrounding hMT+ is specific to limbs or generalizes to other body part images and statistical contrasts.

**Control mapping experiment with larger voxels—**Two subjects participated in the original six category localizer in an additional session where we implemented a data acquisition with voxels eight times as large as our original acquisition (3.75 × 3.75 × 4 mm compared to 1.5 × 1.5 × 3 mm used in the main experiment). The experimental design and exemplars were exactly the same as those detailed in the explanation of the six category experiment in prior sections.

## fMRI Data Collection

**Scanning—**Subjects were scanned on a GE 3-Tesla Signa scanner at the Lucas Imaging Center at Stanford University using a custom-built phased-array, 8-channel surface coil (Nova Medical, Inc. Wilmington, MA, USA). Data were collected over multiple sessions in different days.

**Six category experiment (session one), motion experiment (session one), MST localizer (session five), and body- and body part-selective localizer (session six):** We acquired 12 slices at a resolution of 1.5 × 1.5 × 3 mm (6.75 $mm^3$) using a two-shot T2*-sensitive spiral acquisition sequence (Glover, 1999) (FOV = 192 mm, TE = 30 ms, TR = 1000 ms, flip angle = 77° and bandwidth = 125 kHz). The protocol used a two-shot spiral acquisition sequence, thus the effective TR was 2000 ms. Inplane anatomicals were acquired with the same prescription using a two-dimensional RF-spoiled GRASS (SPGR) sequence (TE = 1.9 ms, flip angle = 15°, bandwidth = 15.63 kHz).

**Six category experiment (session two), motion experiment (session two), and three-position experiment (session four):** We acquired 26 slices at a resolution of 1.5 × 1.5 × 1.5 mm (3.375 $mm^3$) using a two-shot T2*-sensitive spiral acquisition sequence (FOV = 192 mm, TE = 30 ms, TR = 2000 ms, flip angle = 77° and bandwidth = 125 kHz). The protocol used a two-shot spiral acquisition sequence, thus the effective TR was 4000 ms. Inplane anatomicals were acquired with the same prescription using a SPGR sequence (TE = 1.9 ms, flip angle = 15°, bandwidth = 15.63 kHz).

**Visual field mapping (session three):** For the six subjects in the visual field mapping experiment with bar apertures, we acquired 20 slices at a resolution of 2.5 × 2.5 × 2.5 mm (15.625 $mm^3$) using a one-shot T2*-sensitive spiral acquisition sequence (FOV = 220 mm, TE = 30 ms, TR = 1500 ms, flip angle = 71°). For the three subjects in the visual field mapping experiment with checkerboard wedges and rings, we acquired 32 slices at a resolution of 3.125 × 3.125 × 3 mm (29.30 $mm^3$) using a one-shot T2*-sensitive spiral acquisition sequence (FOV = 200 mm, TE = 30 ms, TR = 2000 ms, flip angle = 76°; see Sayres and Grill-Spector, 2008 for details).

**Six category experiment with larger voxels (session seven):** We acquired 36 slices (whole brain) at a resolution of 3.75 × 3.75 × 4 mm (56.25 $mm^3$) using a T2*-sensitive spiral acquisition sequence (FOV = 240 mm, TE = 30 ms, TR = 4000 ms, flip angle = 76° and bandwidth = 125 kHz). Inplane anatomicals were acquired with the same prescription using a SPGR sequence (TE = minimum, flip angle = 45°, bandwidth = 31.25 kHz).

**Anatomical brain volumes—**A high-resolution anatomical volume of the whole brain was acquired with a head coil using a T1-weighted SPGR pulse sequence (TR = 1000 ms, flip angle = 45°, 2 NEX, FOV = 200 mm, resolution of 0.78 × 0.78 × 1.2 mm).

## Data Analysis

Data were analyzed with MATLAB using the mrVista toolbox (http://white.stanford.edu/software).

**Anatomical data—**Anatomical volumes (resolution: 1mm isotropic voxels) were segmented into gray and white matter and from this segmentation we reconstructed the cortical surface for each subject (Wandell et al., 2000). Each subject's data was aligned to their high-resolution anatomical volume, enabling us to compare data across sessions and to visualize activations on the inflated cortical surface.

**Time Course Processing:** Functional data of each session were motion corrected using an affine transformation (Nestares and Heeger, 2000). Time series data were filtered using a temporal high-pass filter with a 1/20 Hz cutoff and then converted to percentage signal change by dividing the time series of each voxel by its mean intensity. Standard general linear model (GLM) analyses were used to create voxel-by-voxel activation maps (Worsley et al., 1997). Data were not spatially smoothed. We estimated the BOLD response

amplitudes for each stimulus category by computing the beta coefficients from a GLM applied to the preprocessed time series of each voxel using as predictors the experimental conditions convolved with the hemodynamic impulse response function used in SPM. In order to examine category selectivity, position sensitivity, and body part selectivity of each limb-selective region of interest (see below), time courses from the six category experiment (session two, independent data), three-position experiment, and body part experiment were extracted from each limb-selective ROI defined from the six category experiment in session one. Data were averaged across hemispheres in each subject and then averaged across subjects. We determined significance of effects across subjects using *t*-tests (when comparing effects relative to another condition or relative to zero, Table 1, *t*Figure 7, Supplemental Figures 2 and 3). To validate the significance of the results, we repeated these statistical analyses with a non-parametric test (Wilcoxon rank sum test). As the significance of the results remained unchanged, we report the statistics resulting from the -tests. When performing analyses of variance (Figure 7) we used a repeated measures 2-way ANOVA with condition and ROI as factors and subject as a repeated measure.

**Region of Interest (ROI) Selection:** Limb-selective ROIs were defined on a subject-by-subject basis using the data from the six category experiment in session one. Five limb-selective clusters were defined based on their distinct anatomical locations with a contrast of limbs > faces, flowers, cars, guitars, and houses ($t > 3$, $p < 0.002$, voxel level, uncorrected, where each condition was equally weighted; Figures 4, 5, and Supplemental Figure 1 show eleven example hemispheres): (1) lateral occipital sulcus/middle occipital gyrus (LOS/MOG; 17/18 hemispheres), (2) inferotemporal gyrus (ITG; 18/18 hemispheres), (3) middle temporal gyrus (MTG; 18/18 hemispheres), (4) occipitotemporal sulcus sometimes extending into the lateral fusiform gyrus (OTS; 16/18 hemispheres), and (5) intraparietal sulcus (IPS; 18/18 hemispheres).

***LOTC anatomical ROI:*** We defined an LOTC anatomical ROI on the gray matter to provide an independent and unbiased way to select voxels for multivoxel pattern (MVP) analyses. This ROI had four anatomical boundaries: LOS (posterior boundary), MTG (anterior boundary), STS (superior boundary), and OTS (inferior boundary). To generate this ROI, we first created a 30mm (diameter) disk ROI on the cortical surface of each hemisphere centered on hMT+ (located in the posterior portion of the ITS). This ROI was then adjusted to exclude the STS and OTS, resulting in an ellipsoidal ROI in LOTC. In each hemisphere, this ROI included all LOTC motion- and limb-selective voxels, as well as visual field maps LO-1/2 and TO-1/2.

**Multivoxel pattern (MVP) analyses examining the relationship between motion, limbs, faces, and cars:** We transformed the time courses from the six category localizer and motion localizer from scanning sessions one and two to the anatomical volume of each subject. This transforms the data into a common reference frame. The MVP for each condition was represented as a vector of length n (where n is the number of voxels in the anatomical LOTC ROI). The MVP represents the spatial activation profile for each condition across the six category and motion experiments separately for each session across the anatomical LOTC ROI. For each voxel, we calculated the amplitude (GLM beta) for each condition (motion, limbs, faces, and cars) relative to the mean beta across these four conditions. We included static images of faces, limbs, and cars in this analysis because each of these conditions robustly activates lateral occipitotemporal cortex, and contains stimuli that move in natural conditions. To examine the reliability of within-condition MVPs across experiments, as well as the relationship between-condition MVPs, we measured the correlation of the MVP for each pairing of stimulus conditions across sessions. This analysis included six of nine subjects because three subjects did not participate in the motion experiment in session two due to experimental constraints. Table 1 summarizes these

correlations. For more details, we orient the reader toward a recent paper examining the relationship between face- and limb-selective activations across both MVP and GLM analysis methods (Weiner and Grill-Spector, 2010).

## RESULTS

### Three limb-selective activations with distinct anatomical locations surrounding hMT+

Using high-resolution fMRI measurements, we first examined the spatial organization of limb-selective and motion-selective responses in LOTC relative to each other in order to test the three scenarios proposed in Figure 1. The first scenario (Figure 1a) is the standard model describing the spatial relationship between the EBA and hMT+, according to which there is one contiguous spherical EBA located posterior (and a bit superior) to, as well as largely overlapping with, hMT+ on the posterior portion of the inferotemporal sulcus (pITS; based on descriptions by Peelen et al., 2006; Downing et al., 2007). The second scenario (Figure 1b, inferred from figures in Spiridon et al., 2006; Pinsk et al., 2009; Orlov et al., 2010; Schwarzlose et al., 2008) suggests that the EBA is organized as a ring surrounding hMT+. This scenario suggests overlap between limb- and motion-selective voxels on the edge of hMT+, but the middle of this activation on the pITS is primarily motion-selective. According to the third scenario (Figure 1c, similar to the anatomical definition of MT and MTc from Tootell and Taylor, 1995), motion- and limb-selective activations are largely non-overlapping with three distinct limb-selective components surrounding hMT+ with separate anatomical locations.

Using GLM contrasts, we determined the spatial organization of limb- and motion-selective activations relative to each other, as well as relative to anatomical landmarks within LOTC. Figures 4a and 5 illustrate examples of this analysis where LOTC limb- and motion-selective voxels are visualized on the inflated cortical surfaces of seven example hemispheres. Limb-selective responses are determined as those LOTC voxels activated by the contrast of limbs > faces, flowers, cars, guitars, and houses from the six category experiment in session one ($t > 3$, voxel level, uncorrected; green in Figures 4a and 5). Motion-selective responses are determined as those LOTC voxels activated by the contrast of moving > static gratings from the motion experiment also in session one ($t > 3$, voxel level, uncorrected; blue in Figures 4a and 5). We refer to these motion-selective voxels as hMT+ because they manifest as one contiguous activation on the ascending limb of the pITS (Dumoulin et al., 2000). As illustrated in Figures 4a and 5, we find evidence for three separate limb-selective activations around the perimeter of hMT+ where each is associated with a distinct anatomical landmark. The first activation is consistently located on the lateral occipital sulcus/inferior portion of the middle occipital gyrus (LOS/MOG) in 17/18 hemispheres (dark green outline in Figures 4a and 5) and is posterior to hMT+. The second activation is consistently located on the inferior temporal gyrus (ITG) in 18/18 hemispheres (yellow outline in Figures 4a and 5) and inferior to hMT+. The third activation is consistently located on the middle temporal gyrus (MTG) in 18/18 hemispheres (red outline in Figures 4a and 5) and anterior to hMT+. Notably, there is no limb-selective activation directly superior to hMT+. As illustrated in Figure 4a, this organization is not restricted to the right hemisphere, but also extends to the left hemisphere (see Supplemental Figure 1 for 4 additional example left hemispheres). Thus, our GLM analyses support the third scenario (Figure 1c), where there are three limb-selective activations in separate anatomical locations with consistent spatial relationships to hMT+ rather than one contiguous EBA overlapping hMT+ (Figure 1a) or a ring of limb-selective activations fully encompassing hMT+ (Figure 1b) because there is no limb-selective activation directly superior to hMT+.

## Limb and motion responses in LOTC are spatially distinct as indicated by both GLM and MVP analyses

Previous studies have illustrated substantial overlap between the EBA and hMT+ with standard GLM analyses (Spiridon et al., 2006; Downing et al., 2007). However, the percentage of overlap has not been quantified. Using the results of our GLM analyses illustrated in Figure 5, we quantified the percentage of limb-selective voxels that overlapped with hMT+ (cyan in Figure 5), separately in each hemisphere and subject. This calculation indicates that only 17.2% ± 2.3% SEM of limb-selective voxels overlapped with hMT+, where there is more overlap between the ITG and hMT+ compared to the overlap between either the LOS or MTG with hMT+ (ITG: 23.5% ± 5.6% SEM compared to LOS: 14.9% ± 3.6% SEM and MTG: 13.0% ± 3.4% SEM). Of course, the percentage is based on the statistical threshold used to define activations. To circumvent this limitation, MVP analyses in an anatomically defined ROI enable a threshold independent examination of the spatial relationship among distributed responses (Peelen and Downing, 2007; Weiner and Grill-Spector, 2010).

We next examined the relationship of limb-, motion-, face-, and car-MVPs both within and across conditions by correlating the distributed response patterns to these stimuli from each independent session of the six category experiment (sessions one and two) and motion experiment (sessions one and two) in an anatomically defined LOTC ROI (see Materials and Methods). There are three possible outcomes to this analysis. First, there may be an anticorrelated relationship between limb- and motion-MVPs. This would indicate that distinct subsets of LOTC voxels respond preferentially to either motion or limbs, supporting largely nonoverlapping sets of voxels for processing motion and limb information. Second, there may be a positively correlated relationship between limb- and motion-MVPs. This would indicate that voxels preferring limbs also prefer motion, suggesting that a common set of voxels prefer both conditions. Finally, there may be a decorrelated relationship between limb- and motion-MVPs, which would indicate independent information for these two conditions. That is, the degree to which a voxel prefers limbs is uninformative about the degree to which it prefers motion.

MVP analyses show that within-condition MVPs are reproducible across experiments (significantly positive correlations, $ts(5) > 3.91$, $ps < 10^{-3}$, Table 1). Between-condition correlations illustrate common sets of voxels coding face- and car-MVPs (significantly positive correlations, $t(5) = 2.10$, $p < .04$) and no relationship between face- and limb-MVPs (correlations not significantly different than zero, $t(5) = .52$, $p=.62$). Notably, the correlation between limb- and motion-MVPs is significantly negative ($t(5) = 7.45$, $p < 10^{-4}$). These anticorrelated activation patterns for limbs and motion across LOTC indicate spatially distinct responses for limbs and motion. Similarly, face- and motion-MVPs are anticorrelated. This effect is stronger than the anticorrelation for limb- and motion-MVPs ($t(5) = 2.3$, $p < .04$) because face-selective voxels in LOTC (which are typically located separately on the inferior occipital gyrus and the posterior superior temporal sulcus) are farther away from hMT+ compared to limb-selective voxels (see Supplemental Figure 1 in Weiner and Grill-Spector, 2010). Taken together, both MVP and GLM analyses indicate that responses for motion and limbs are spatially distinct in LOTC.

## Three distinct LOTC limb-selective activations on separate visual field maps

As there are several visual field maps in LOTC, we used these maps as independent measurements to either verify or refute our parcellation of limb-selective activations based on anatomical location and spatial relationship to hMT+. Visual field mapping is a useful technique because the representation of the visual field is a fundamental property that is used to dissociate visual areas in both the human and monkey brain. Moreover, it constrains

the criteria for deciding whether to split or group activations together. If limb-selective activations overlap discontinuous representations of the visual field (i.e. they skip a hemifield representation), then they should be taken separately. However, if an activation spans a continuous representation of the visual field, then this activation could be grouped together. For example, researchers consistently define hMT+ based on its motion selectivity measurement even though it contains two successive visual field maps.

In all 18 hemispheres, we defined visual field maps in LOTC and up the dorsal stream extending into the IPS using both polar angle and eccentricity measurements (Figure 4b-c for an example subject). We defined LO-1/2, TO-1, V3ab, and V7 in all hemispheres and TO-2 in 16/18 hemispheres. In order to examine the accuracy of the parcellation of LOTC limb-selective activations based on anatomical location and spatial relationship to hMT+, we overlaid the boundaries of both LOTC and IPS visual field maps over the limb- and motion-selective activations (green and blue in Figures 4a and 5, respectively), on the inflated cortical surface of each hemisphere. Figure 5 illustrates the resulting visualizations in six example hemispheres, where the limb-selective LOS/MOG, ITG, and MTG are outlined in green, yellow, and red, respectively. The outlines for each visual field map are illustrated, with a dotted line extending from the TO fovea (depicted by an asterisk) indicating the shared upper field representation between TO-1 and TO-2. This boundary divides hMT+ in nearly all hemispheres (15/18) as previously reported (Amano et al., 2009). The three cases where this did not occur were a result of either an undefined TO-2 (two hemispheres, e.g., Subject S1 in Figure 5), or hMT+ largely falling within TO-2 (Subject S2 in Figure 5).

As illustrated in Figure 5 and summarized in Figure 6, the limb-selective LOS/MOG partially overlaps with TO-1 in nearly all hemispheres (16/17 hemispheres; Figure 6a, dark gray). In Figure 5, the location of the LOS/MOG (outlined in dark green) is always posterior to the dotted line that denotes the TO-1/TO-2 boundary and largely overlaps with the shared lower field representation of LO-2/TO-1. However, there is variability as to the number of visual field maps that the limb-selective LOS/MOG traverses. It is not the case that the LOS/MOG coincides only with TO-1. It falls just within TO-1 in about one-third of the hemispheres (6/17; S5 and S6 in Figure 5 are two such examples), overlaps with LO-2/TO-1 in about half of the hemispheres (7/17; S1, S2, and S4 in Figure 5 are three such examples), and extends from LO-1 to TO-1 in a minority of hemispheres (3/17; S3 in Figure 5 is one such example), and does not reach TO-1 in only one hemisphere (this example is illustrated in Figure 4a). Thus, as summarized in Figure 6, the LOS/MOG activation overlaps with LO-2/TO-1, seldomly extends into LO-1, and never extends into TO-2.

On the other hand, the limb-selective MTG overlaps with TO-2 in a majority of hemispheres (11/16). In Figure 5, the location of the MTG (outlined in red) is anterior to the dotted line indicating the TO boundary and tends to overlap with a separate lower visual field representation on the anterior end of TO-2. Like the more posterior LOS/MTG activation, the MTG rarely overlaps with just one visual field map. In fact, the MTG overlaps with just TO-2 in a minority of hemispheres (2/16; S4 in Figure 5 is an example; Figure 6a, black). The limb-selective MTG overlaps with TO-2 and extends anteriorly outside known visual field maps in more than half of the hemispheres (9/16; S3, S5, and S6 in Figure 5 and S2 in Figure 4a are four such examples), and only extends anterior to TO-2 in about one-third of the hemispheres (5/16; S2 in Figure 5 is one example). Notably, there are no limb-selective voxels on the upper field representation shared between TO-1 and TO-2, which illustrates that 1) the center of hMT+ is spared of any limb-selective voxels and 2) the limb-selective LOS/MOG and MTG overlap two separate representations of the lower visual field.

The limb-selective ITG, which is located inferior to hMT+, largely overlaps with the parafoveal representation of the TO cluster in more than three-quarters of the hemispheres

measured (14/18; Figure 6a, white). In Figure 5, the TO fovea is indicated by an asterisk and the ITG (outlined in yellow) typically overlaps with the TO foveal representation (S3, S5, and S6 in Figure 5 and S2 in Figure 4c are four examples) and extends into the parafoveal representation (S1, S2, and S4 in Figure 5 are three such examples).

The results of this analysis indicate that though these limb-selective activations are defined based on the same statistical contrast of higher BOLD responses to images of limbs compared to images from other categories, they should be divided into three separate activations based on their 1) distinct anatomical location, 2) differential spatial relationship relative to hMT+, and 3) overlap with separate and discontinuous visual field maps.

## Limb-selective IPS overlaps with V7

We identified another region in visual cortex in which a limb-selective activation is both adjacent to a motion-selective activation as well as overlaps a particular visual field map. Specifically, there is a limb-selective activation in the posterior portion of the IPS that overlaps with V7 in nearly all hemispheres (17/18, see Figure 5 and Figure 6b). Like the LOTC limb-selective activations, there is also variability in the degree to which this activation extends either more posteriorly into the peripheral representation of V3a or more anteriorly into IPS-1. The limb-selective IPS falls only in V7 in over half of the hemispheres (10/18; S1 and S5 in Figure 5 are two examples), overlaps with V7 and extends into the shared upper field representation with V3a in about one-fifth of the hemispheres (4/18; S3 and S6 in Figure 5 are two examples), overlaps with V7 and extends into the shared lower field representation with IPS-1 in one hemisphere, or overlaps with V7, V3a, and IPS-1 in two hemispheres (S2 and S4 in Figure 5). Interestingly, our data also illustrate a close correspondence between the limb-selective IPS and a nearby motion-selective activation previously referred to as vIPS (Orban et al., 2006 for review), which is distant from a separate motion-selective activation located near the fovea shared between V3a and V3b. This vIPS motion-selective activation is consistently located posterior to the limb-selective IPS activation (see S2-S6 in Figure 5) and tends to overlap V3a and the posterior portion of V7.

## Consistent category selectivity in the LOTC limb-selective activations

To examine the functional properties within these regions, we conducted two additional measurements where the first examined the category selectivity using the independent data from the six category experiment in session two and the second examined the position sensitivity based on responses to limbs presented either centrally or 4º to the left or right of fixation (see Figure 2 and Materials and Methods for details).

We first measured the mean ROI responses across subjects from the second session's six category experiment. The LOTC limb-selective responses illustrate similar category selectivity with higher responses to limbs compared to other categories, indicating that the profiles of limb-selective responses are consistent across sessions one and two. Activations are strongest to limbs, second-best to faces, and lowest to houses (Supplemental Figure 2). To quantify category-selectivity within each region, we calculated *t*-values of contrasts relating limbs to other categories (limbs > flowers, cars, guitars, and houses) as well as limbs to faces (limbs > faces). This analysis indicates that the three limb-selective activations illustrate comparable limb selectivity. However, there is decreasing face selectivity (*t*-value of faces > flowers, cars, guitars, and houses) from the LOS to the ITG to the MTG (Figure 7a), where there is positive face-selectivity in the limb-selective LOS/MOG and ITG (all *t*s > 2.3 compared to 0, all *p*s < .03), but not in the MTG (t(8)=1.08, $p = .16$).

### Decreasing contralateral bias and increasing foveal bias from the limb-selective LOS/MOG to the limb-selective MTG

Since TO-1 has smaller population receptive field sizes than TO-2 (Amano et al., 2009; Winawer et al., 2010), we hypothesized that the limb-selective LOS/MOG, which overlaps TO-1, would illustrate stronger retinotopic modulations than the limb-selective MTG, which overlaps TO-2, and also extends outside known visual field maps. To examine this hypothesis, we compared responses to upper and lower limbs presented foveally, 4° to the right, and 4° to the left of fixation (three position experiment, see Materials and Methods and Figure 2d), predicting that the limb-selective LOS/MOG would show a stronger contralateral bias than the MTG activation. We calculated the contralateral bias (contralateral > ipsilateral) as well as the foveal bias (foveal > contralateral) in each of our three limb-selective LOTC activations. This analysis was done in two ways: using a *t*-contrast (Figure 7b) or by comparing the average signal magnitudes across conditions (Supplemental Figure 2b) and yielded similar results. Results show that the limb-selective LOS/MOG illustrates a significantly higher contralateral than foveal bias for the presentation of limb images (Figure 7b; contralateral > foveal, $t(5) = 2.07$, $p < .05$), while the ITG and MTG did not. A two-way repeated-measures ANOVA using as factors region (LOS/MOG, ITG, and MTG) and position bias (contralateral, foveal) yielded a significant interaction ($F(2,10) = 5.99$, $p < .02$), indicating that there is a decreasing contralateral bias and an increasing foveal bias from the LOS/MOG into the ITG and to the MTG. Furthermore, the differential position sensitivity is not due to overlap with hMT+ because the same pattern of results is apparent when excluding voxels that overlap with hMT+ (Supplemental Figure 2b), illustrating that the three LOTC limb-selective activations differ in their position sensitivity.

### Foveal bias in limb-selective OTS and negative face selectivity and contralateral bias in limb-selective IPS

As we identified two additional limb-selective activations outside LOTC in the IPS and OTS (see Figure 5 and Materials and Methods for ROI delineations), we also examined the functional properties of these additional activations. As expected, these activations exhibit consistent limb selectivity (Supplemental Figure 3a). However, the LOTC limb-selective activations illustrate about 1.5 times as much limb-selectivity as the OTS and about two times as much limb-selectivity as the IPS (IPS is significantly less than each limb-selective activation; all $t$s > 3.45, all ps < $10^{-3}$; pairwise comparisons, Bonferroni corrected for multiple comparisons). Interestingly, the limb-selective IPS is the only limb-selective activation illustrating negative face selectivity (Supplemental Figure 3a; $t(8)=2.45$, compared to 0, $p < .02$), while the other limb-selective activations either prefer faces over other categories (LOS/MOG and ITG) or illustrate comparable responses (MTG). Finally, unlike the limb-selective LOTC activations, the OTS shows a stronger foveal bias than contralateral bias ($t(5) = 2.08$, $p < .05$; Supplemental Figure 3b), while the limb-selective IPS exhibits a stronger contralateral than foveal bias $t(4) = 2.49$, $p < .03$) similar to the LOS/MOG. Taken together, the current data support a distributed network of limb-selective activations located ventrally (OTS), laterally (LOS/MOG, ITG, MTG), and dorsally (IPS) in consistent anatomical locations and spatial relationships to visual field maps.

### Functionally-defined areas MT and MST separate LOTC limb-selective activations

We also examined the relation of our limb activations to separate hMT+ subcomponents. hMT+ is known to contain at least two functional subcomponents, a posterior component corresponding to area MT, and a more anterior component, area MST. Consequently, we localized MT and MST using a separate MST localizer experiment (see Materials and Methods) and examined their spatial relationship to the limb-selective LOS/MOG, ITG, and MTG activations, respectively. As illustrated in Figure 8 (left) on the inflated cortical

surface, there is a consistent spatial relationship among areas MT and MST with each of the three LOTC limb-selective activations where (1) area MT (blue) is located anterior to the limb-selective LOS/MTG (green), (2) both MT and MST (magenta) are superior to the limb-selective ITG (yellow), and (3) MST is posterior to the limb-selective MTG (red). This evident spatial distinction among activations is also clear on the volume with example sagittal, coronal, and axial slices from these two subjects (Figure 8, right). Results of this analysis indicate that the spatial relationship among the limb-selective activations and MT/MST is the same as the spatial relationship among the limb-selective activations and visual field maps TO-1/2, which replicates recent results indicating that visual field maps TO-1/2 correspond to the functional subdivisions of hMT+, MT and MST, respectively (Amano et al., 2009). That is, the LOTC limb-selective activations do not substantially overlap either MT or MST. Taken together, the initial parcellation of the limb-selective activations based on anatomy and spatial relationship to hMT+ is verified with both independent data measuring visual field maps in LOTC, and with the functional subdivisions of hMT+ (areas MT and MST).

### Crescent organization surrounding hMT+ is consistent across a span of three years and different types of stimuli used to localize body- and body part-selective LOTC voxels

In the present study, we contrasted neural responses to images of limbs relative to images from an array of different categories in order to localize LOTC limb-selective voxels. In order to relate the organization observed presently to reports which used images of headless bodies to localize the EBA (Supplemental Table 1), we scanned three of our subjects in the original six category localizer as well as a new version using images of headless bodies instead of limbs. This manipulation allows the direct comparison of maps produced by headless bodies to maps produced by limbs relative to the same control stimuli. We also conducted a third experiment on these subjects in which they viewed images of different body parts (torsos, legs, and hands), headless bodies, faces, houses, and chairs to examine the LOTC organization using completely different stimuli.

The crescent organization of limb-selective voxels surrounding hMT+ is reproduced three years later, as illustrated in Figure 9a (middle, left). Further, the contrast of headless bodies vs. other categories (Figure 9a, middle right) shows that many of these voxels fall within the original limb-selective ROIs and hMT+ is largely spared of any voxels selective for headless bodies. We further examined the limb and body selectivity across the union of the original limb-selective ROIs because there was no difference in limb selectivity in our original measurements (Figure 7a, limbs > others). To determine selectivity, we calculated the average *t*-value in two ways: limbs > other categories and headless bodies > other categories. There is no difference in the average *t*-value for headless bodies or limbs (Figure 9a, far right) indicating that studies using images of headless bodies in their EBA localizers will also reproduce this crescent organization.

We next tested how changing all exemplars used to localize LOTC voxels would affect the organization. Using a statistical contrast of legs, torsos, headless bodies, and hands relative to faces, houses, and chairs, there is a large correspondence between the original limb-selective activations and those voxels that prefer different parts of the body (Figure 9b for three example subjects; Supplemental Figure 1b for left hemisphere). That is, voxels that are selective for both body and body parts fall within the original ROIs. However, there are additional voxels that arise from this new contrast as one would expect when changing both the experimental and control exemplars (Orlov et al., 2010). Importantly, the body and body-part selective voxels do not extend into hMT+, but rather extend posteriorly into the LOS and do not form a spherical EBA encompassing hMT+.

Finally, using the original ROIs, we extracted the timecourses from the body part experiment and calculated the average *t*-value in each ROI using chairs, houses, and faces as a baseline. As illustrated in Figure 9b (far right), preference for images of different body parts varies across ROIs, which replicates recent findings (Orlov et al., 2010; Bracci et al., 2010).

It should be noted that when more specific contrasts are used, such as hands > bodies, torsos, legs, faces, chairs, and houses, we extend prior results reporting focal activations selective for images of a particular body part, such as a hand-selective activation on the MTG (Supplemental Figure 4a). However, when contrasting activations to specific body parts relative to non-body images (such as hands > faces and houses), a constellation of activations surrounding hMT+ is found rather than a singular focal activation (Supplemental Figure 4b).

Taken together, a consistent factor in our measurements is that voxels selective for images of the human body, body parts, and limbs in LOTC do not encroach into the center of hMT +. Furthermore, using anatomical landmarks and the spatial relationship to hMT+ to define the original limb-selective ROIs accurately predicts functional differences across these ROIs three years later.

## Anatomical landmarks and hMT+ are sufficient to parcellate limb-selective LOS/MOG and MTG activations even with standard fMRI

Is high-resolution fMRI necessary to separate these LOTC limb-selective activations from one another and hMT+? To address this question, we scanned two subjects in the six category and motion experiments with functional voxels eight times as large as our original scanning acquisition (3.75 × 3.75 × 4mm compared to 1.5 × 1.5 3mm). In Figure 10, we illustrate one example hemisphere with three noteworthy findings. First, without segmenting gray from white matter, it is hard to separate the three separate limb-selective components from one another and the organization resembles a contiguous 'extrastriate body area' even without spatial smoothing (Figure 10a). Second, when the same activation is restricted to gray matter and projected onto the inflated cortical surface (Figure 10b), it is rather easy to see the three separate components (LOS/MOG, ITG, and MTG in green, yellow, and red, respectively) surrounding hMT+ (blue). Third, just by adding the location of hMT+, it is possible to segregate the LOS/MOG from the MTG even on the brain volume (compare two rightmost panels in Figure 10c), as hMT+ further separates the two components, whereby the LOS/MOG is posterior to hMT+ and the MTG is anterior to hMT+. As the limb-selective ITG is immediately inferior to hMT+ (compare two rightmost panels in Figure 10c), and is located on a separate gyrus, it can be separated from the other activations using the sagittal view. However, identifying the limb-selective ITG is difficult on the unsegmented brain volume even with anatomical and functional landmarks. Using cortical surface visualizations can make this distinction much more straightforward (as in Figure 10b).

Figure 10 can serve as a two-step guide for researchers using standard-resolution fMRI to divide the limb-selective LOS/MOG from the MTG as this division is clear across scanning resolutions and visualizations. First, anatomical location is a reliable predictor for the localization of these separate LOTC limb-selective activations. Second, identifying hMT+ aids this parcellation. Thus, data acquisition with larger voxels and brain volume visualizations should not deter researchers from separating LOTC limb-selective activations. Rather, by determining the anatomical location of activations and conducting just a 3.5 minute hMT+ localizer scan, it is possible to separate the limb-selective LOS/MOG from the limb-selective MTG. Using brain volume visualizations, this separation is most easily observed on sagittal and axial slices.

## DISCUSSION

The current study examines the fine-scale spatial organization of limb- and motion-selective responses in lateral occipitotemporal cortex (LOTC), and reports three separate limb-selective activations organized in a crescent surrounding the human MT+ complex (hMT+), rather than one contiguous extrastriate body area (EBA) overlapping hMT+, supporting the organization in Figure 1c. Each limb-selective activation is located relative to distinct anatomical landmarks corresponding to separate portions of visual field maps TO-1 and TO-2, as well as motion-selective areas MT and MST. This relationship is summarized in the schematic in Figure 11. Specifically, the limb-selective LOS/MOG is located posterior to functional area MT on the lower field representation shared between LO-2 and TO-1. The limb-selective ITG most consistently overlaps with the inferior portions of both areas MT and MST (visual field maps TO-1 and TO-2, respectively), on the foveal and parafoveal representations of the TO cluster. The limb-selective MTG is anterior to MST, overlapping the lower field representation of TO-2 and extending outside known visual field maps. Notably, no limb-selective voxels are located in the center of the TO cluster (the center of hMT+), which is the location of the shared upper field representation between TO-1 and TO-2. In addition to overlapping separate visual field maps, the limb-selective LOTC activations are also functionally dissociable based on their position sensitivity. In particular, the limb-selective LOS/MOG illustrates a higher contralateral than foveal bias for stimulus presentation, whereas the limb-selective MTG and ITG do not (Figure 7c). Finally, this relationship between limb-selective activations and visual field maps continues to parietal cortex where there is a correspondence between a limb-selective activation on the posterior portion of the IPS and V7.

We next consider these results in the context of (1) additional suggested visual field map parcellations within LOTC, (2) the organization of cortex surrounding MT in humans and monkeys, (3) other suggested functional differences between LOS and MTG activations, and (4) the transition of visual information into an action output in IPS. Finally, we elaborate on the implications of these results in defining brain areas based on category selectivity alone.

### Parcellation of limb-selective activations is consistent with additional definitions of LOTC visual field maps

As limb selectivity (and category selectivity in general) is a rather uncontrolled and discontinuous stimulus space, we used visual field maps as independent measurements to support our parcellation of limb-selective activations based on anatomical location and spatial relationship to hMT+. While visual field maps are a fundamental property of visual cortex, presently there are several suggested organizations of visual field maps spanning the region anterior to V3d and extending through hMT+ (Amano et al., 2009; Barton and Brewer, 2010; Hansen et al., 2007; Huk et al., 2002; Kolster et al., 2010; Larsson and Heeger, 2006; Pitzalis et al., 2010). In the current study, we utilized the LO-1/2 and TO-1/2 parcellation scheme of Larson and Heeger (2006) and Amano and colleagues (2009) based on the visual field mapping stimuli we have used (see Materials and Methods). Nevertheless, our parcellation of LOTC limb-selective activations also fits with other recently proposed organizations, as all reports consistently identify only one foveal representation on the pITS and the limb-selective activations reported here are organized in a consistent manner relative to this fovea (Figure 11). A recent report suggests that the parafoveal representation on the ITG may include two additional maps measured with spatiotemporally optimized stimuli (pV4t and pFST, Kolster et al., 2010). Thus, the limb-selective ITG is likely to overlap these maps, which we were unable to measure with the current visual field mapping stimuli. However, we are not opposed to further parcellation of these limb-selective activations.

### Crescent organization surrounding MT: Human

The current data indicate that limb-selective and motion-selective activations are spatially distinct from one another and further, that the limb-selective activations are organized in a crescent-shape around hMT+ with no limb-selective activation directly superior to hMT+. The present parcellation is based on the anatomical location of the limb-selective activations, their spatial relationship relative to other known high-level visual activations and visual field maps, as well as differences in the functional properties of these activations. In support of this parcellation, additional findings suggest that there are also underlying anatomical differences between human MT and its surrounding cortex. Critically, anatomical studies in humans show that MT is more densely myelinated than the crescent-shaped surrounding cortex, which is recognized as a distinct region, MT crescent (MTc; Tootell and Taylor, 1995). Thus, we speculate that the present findings of three limb-selective activations organized in a crescent surrounding hMT+ may be a direct reflection of underlying anatomical differences between area MT and its surrounding cortex. Future studies examining the correspondence between anatomical and functional organization would be critical to examine this LOTC organization in detail using recently developed non-invasive methods (Walters et al., 2003).

### Crescent organization surrounding MT: Monkey

The crescent organization surrounding hMT+ demonstrated in the current study is similar to the spatial organization of separate cortical areas surrounding area MT in monkeys. The underlying anatomy surrounding MT in old and new world monkeys illustrates a distinct crescent formation. Some groups refer to the full crescent as a distinct area MTc (Kaas and Morel, 1993; Stepniewska et al., 2005; Tootell and Taylor, 1995), while others subdivide this crescent into a V4t component and an FST component based on anatomical and functional criteria, as well as differences in cortico-cortical connections (Desimone and Ungerleider, 1986; Felleman and Van Essen, 1991). Thus, the parcellation of the areas surrounding MT in the monkey seems to be analogous to the spatial organization of our limb-selective activations relative to MT and MST in the human, where the posterior limb-selective LOS/MOG is spatially congruous to monkey V4t, the inferior limb-selective ITG is spatially congruous to FST, and the limb-selective MTG is spatially congruous to the posterior component of STP. However, an open question remains: Where are limb-selective activations located in monkey temporal cortex?

To date, a handful of fMRI studies in monkeys reported body part-selective activations within inferotemporal cortex in areas TEO and TE (Bell et al., 2009; Pinsk et al., 2009; Pinsk et al., 2005; Tsao et al., 2003), which are cortically distant from areas MT and MST located in the STS. Electrophysiology studies have also documented hand-selective neurons in TE (Desimone et al., 1984; Gross et al., 1969; Gross et al., 1972) and neurons sensitive to both body form and direction of motion within the anterior portion of STP (Oram and Perrett, 1996). Thus, a key difference across species seems to be that static images of limbs and body form activate mostly inferotemporal regions in the monkey, but in humans they activate a network of activations ventrally in the OTS (Peelen and Downing, 2005; Schwarzlose et al., 2005; Weiner and Grill-Spector, 2010), laterally surrounding hMT+, and dorsally in the IPS. An open question remains as to why the crescent organization of human limb-selective activations around hMT+ observed here seems to spatially match the organization of V4t, FST, and STP in the monkey, yet the body-selective activations in monkey fMRI studies are distant from these areas, largely restricted to areas TEO and TE. Future monkey fMRI studies can directly address this question by determining potential homologies and differences across species via examination of the spatial organization of high-level visual activations (including those involved in processing bodies and faces that have been observed in both species) relative to visual field maps and MT.

### Functional differences between limb-selective activations on the LOS/MOG and MTG

The current study demonstrates that the limb-selective LOS/MOG, ITG, and MTG are functionally dissociable based on position sensitivity (Figure 7) and preferences to images of particular body parts (Figure 9). Previous neuroimaging studies have also illustrated functional dissociations between the LOS/MOG and MTG within either the visual modality alone or across sensory domains for both visuo-motor and visuo-tactile processing.

Within the visual domain, Bracci and colleagues report an activation on the LOS selective for static images of hands relative to an array of body part and other control images, and a separate posterior body part-selective activation that does not show a clear preference for hands (Bracci et al., 2010). Our high-resolution measurements in individual subjects extend this finding by illustrating a hand-selective activation on the MTG not the LOS (Supplemental Figure 4). When re-visiting Figure 2 in Bracci et al. (2010), which illustrates single subject activations on axial slices, the hand-selective activation is also located on the MTG. This is an important distinction because we show that two well-known functional areas, MT and MST, with vastly different functional properties are located between the LOS and MTG.

A recent study extended this finding of a hand-selective region by illustrating a topographic organization of the human body in LOTC with distinct clusters showing preferences for different body parts (Orlov et al., 2010). We relate two findings from their study to the present results. First, the upper limb representation observed by Orlov et al. (2010) is depicted as a crescent from the MTG to the ITG and extending posteriorly to the LOS (Figure 2 in Orlov et al.), which is consistent with our results (Figures 4, 5, 8, 10-11, and Supplemental Figure 1). Second, the authors report a visuo-motor correspondence, where regions responding to the visual presentation of a particular body part are also activated by unseen movements of that body part, suggesting that LOTC may represent information across sensory domains.

Consistent with this notion of bimodal processing in LOTC, Dinstein and colleagues (2008) illustrate that the LOS is activated for observed hand movements, while a region similar to the limb-selective MTG is activated during executed hand movements. Such a distinction is suggestive of a further functional dissociation between the LOS and MTG based on the visual coding of an observed action in the LOS and executed actions within the MTG. Further, a recent study illustrated that the MTG is also involved in coding the rationality of observed movements, suggesting that the MTG activation may not just be involved in the motor aspect of the executed movement, but also in the visual coding of the feasibility of the movement (Jastorff et al., 2010).

In the visuo-tactile domain, Beauchamp and colleagues reported that human MST, but not MT, responds to tactile stimulation of the hand, but not the foot (Beauchamp et al., 2007) and that distinct MST multivoxel patterns of response correspond to touches of the hand compared to the foot (Beauchamp et al., 2009). Integrating the present findings to the studies conducted by Beauchamp and colleagues, it raises the question whether the limb-selective MTG is involved in processing tactile stimulation of the hand. Future studies can examine visuo-tactile processing across the separate LOTC limb-selective activations.

Taken together, there is substantial evidence for functional dissociations between the LOS and MTG within either the visual modality alone based on position and body part selectivity, or across sensory domains for visuo-motor and perhaps visuo-tactile processing. These findings suggest that the MTG is potentially involved in more combinatorial processing across domains while the ITG and LOS are involved in visual processing, but not multisensory integration.

### Limb-selective IPS: Transition of visual input to action output?

In addition to the series of LOTC limb-selective activations, we also illustrate a consistent limb-selective activation in the posterior IPS most consistently traversing the peripheral representation of V3a into V7. A recent study suggests that this limb-selective IPS may actually represent two separate activations, one for the static presentation of lower limbs in V3a and one for upper limbs anterior to V3a in the posterior IPS (Orlov et al., 2010). We propose that the limb-selective IPS observed here is one of a transitional stage between converting visual inputs into action outputs, whereas IPS-1/2 and the anterior IPS are more involved in the limb-related actions themselves.

Consistent with this idea, several recent studies provide evidence indicating that the posterior IPS is involved in the observation of limb movement, while more anterior IPS regions are involved in the execution of limb movement. Specifically, either viewing the hand during self-induced reaches or observing videos of hand actions activates the posterior IPS, while both self-induced reaches and hand actions without viewing the hand activate the anterior IPS (Dinstein et al., 2008; Filimon et al., 2009). Furthermore, when directly measuring reach-related activity in IPS visual field maps, IPS-2, not V7, illustrates the highest preference for conducted reaches (Levy et al., 2007). Thus, cumulative results from several studies suggest that activations in posterior IPS near the location of V7 and the limb-selective IPS reported here are more consistently activated when observing hand or reaching movements rather than when solely executing them.

Though we do not presume any homologies to the monkey, V7 in humans has been proposed by Tootell and colleagues (Tootell et al., 1998) to correspond to the dorsal prelunate (area DP) in monkeys based on its spatial location relative to V3a. In monkeys, DP is thought to be involved in visual processing (Andersen et al., 1985; Andersen et al., 1985; Felleman and Van Essen, 1991; May and Andersen, 1986), and the coding of visually guided reaches rather than the movement associated with the reaches themselves (Heider et al., 2010). Thus, the human limb-selective IPS overlapping V7 shares more functional and spatial attributes with DP than with other monkey parietal areas involved in limb actions. Future human fMRI experiments are needed in order to dissociate the visual processing associated with limb movement from the resulting action across IPS visual field maps.

### Category selectivity is not a stringent enough criterion to define a brain area

In the current study, we report that there is not one extrastriate body area within LOTC. Rather, there are a series of functionally dissociable limb-selective activations located in distinct anatomical locations with consistent spatial relationships to both hMT+ and known visual field maps. These findings of multiple limb-selective activations located in separate anatomical locations throughout LOTC, IPS, and OTS, with a consistent spatial relationship to other high-level visual activations and visual field maps argue against the notion that the human body is represented by a domain-specific module – the EBA (Kanwisher, 2010) – and instead support a sparsely-distributed network of body representation that we have recently proposed (Weiner and Grill-Spector, 2010).

The definition of category-selective areas is a pressing issue in the field of high-level vision because the space of categories is difficult to define or comprehensively measure in a single experiment. Additionally, it is hard to control for low-level visual features, variability, complexity, and cognitive knowledge associated with a putative category space. Nonetheless, there are multiple brain 'areas' that have been defined based solely on category preference. For example, a commonly used EBA localizer contrasts brain responses to images of headless bodies compared to those responses to images of chairs (Downing et al., 2007; Supplemental Table 1). While this contrast produces reliable activations in LOTC

across subjects and research groups, such a stimulus set is not much of an operationalized improvement from the set of stimuli used more than 30 years ago to measure the properties of face-selective and hand-selective neurons relative to unconventional control stimuli such as toilet brushes (Gross, 2008). We do not intend to imply that our present localizer is better. Instead, we argue that detecting a reliable cluster of voxels resulting from contrasting brain responses to images from one category relative to responses to a handful of other categories is an insufficient criterion to define a brain area. Rather, we propose that several additional criteria need to be met in order to parcellate category-selective activations.

We propose that anatomy, spatial relationship to well-known activations, representation of the visual field, and differences in functional properties are all necessary factors to consider when deciding to separate one brain activation from another. Using these criteria has been productive in other parts of the brain such as the IPS (in the present study) and ventral temporal cortex in a previous study (Weiner and Grill-Spector, 2010). Specifically, we demonstrated that the so-called fusiform face area (Kanwisher et al., 1997) is actually composed of two distinct components located on different anatomical locations along the fusiform gyrus where each cluster illustrates a consistent spatial relationship to the limb-selective OTS and ventral visual field maps hV4 and VO-1/2 (Weiner and Grill-Spector, 2010). Without considering these multiple criteria and continuing to include all limb-selective LOTC voxels as a single category-selective body area irrespective of their precise anatomical location and how they are organized relative to other high-level visual activations, researchers will measure responses across heterogeneous neural populations with differing functional properties (as we have demonstrated in this study). As a consequence, researchers may misinterpret the function and characteristics of the underlying neuronal populations and in turn, generate misguided theories regarding the organization of human LOTC and high-level visual cortex in general.

In addition to the factors of anatomical location, topography, and function used here to parse activations, cytoarchitecture and connectivity measurements have also been used to delineate visual areas in the monkey for more than four decades (Desimone and Ungerleider, 1986; Felleman and Van Essen, 1991 are two such examples). Using non-invasive techniques in humans, future researchers may be able to determine additional properties of anatomical organization using high-resolution structural MRI (e.g. cortical lamination, Walters et al., 2003) and connectivity using diffusion tensor imaging (Dougherty et al., 2005; Sherbondy et al., 2008). These measurements will provide additional evidence to determine which functional activations should be considered visual areas. Until then, category-selectivity is an insufficient organization principle to define brain areas, as it is a single measurement in an uncontrolled and discontinuous stimulus space. Collectively as a field, we should work toward building a better localizer for operationalizing the category space and to shy away from referring to current category-selective activations as 'areas' because they are not determined with sufficiently rigorous criteria as has historically been used to parcellate visual areas.

## Supplementary Material

Refer to Web version on PubMed Central for supplementary material.

## Acknowledgments

This work was supported by National Eye Institute 1R21EY017741; NSF BCS 0617688, NSF BCS 0920865, and Whitehall Foundation 2005-05-111-RES grants to KGS. We thank Rory Sayres for help with data collection, Jon Winawer, and Nathan Witthoft for comments on the manuscript, as well as Anthony Wagner and Brian Wandell for useful conversations. We thank Paul Downing, Marius Peelen, Tanya Orlov, and Udi Zohary for headless body and body part stimuli to directly compare our data to their measurements.

## References


Amano K, Wandell BA, Dumoulin SO. Visual field maps, population receptive field sizes, and visual field coverage in the human MT+ complex. J Neurophysiol. 2009; 102:2704–2718. [PubMed: 19587323]

Andersen RA, Asanuma C, Cowan WM. Callosal and prefrontal associational projecting cell populations in area 7A of the macaque monkey: a study using retrogradely transported fluorescent dyes. J Comp Neurol. 1985; 232:443–455. [PubMed: 3980763]

Andersen RA, Essick GK, Siegel RM. Encoding of spatial location by posterior parietal neurons. Science. 1985; 230:456–458. [PubMed: 4048942]

Barton, B.; Brewer, AA. Pinwheel cartography: A fundamental organizing principle of the human visual system. Society for Neuroscience; San Diego, CA: 2010.

Beauchamp MS, Laconte S, Yasar N. Distributed representation of single touches in somatosensory and visual cortex. Hum Brain Mapp. 2009; 30:3163–3171. [PubMed: 19224618]

Beauchamp MS, Yasar NE, Kishan N, Ro T. Human MST but not MT responds to tactile stimulation. J Neurosci. 2007; 27:8261–8267. [PubMed: 17670972]

Bell AH, Hadj-Bouziane F, Frihauf JB, Tootell RB, Ungerleider LG. Object representations in the temporal cortex of monkeys and humans as revealed by functional magnetic resonance imaging. J Neurophysiol. 2009; 101:688–700. [PubMed: 19052111]

Boussaoud D, Desimone R, Ungerleider LG. Visual topography of area TEO in the macaque. J Comp Neurol. 1991; 306:554–575. [PubMed: 1712794]

Bracci S, Ietswaart M, Peelen MV, Cavina-Pratesi C. Dissociable neural responses to hands and non-hand body parts in human left extrastriate visual cortex. J Neurophysiol. 2010; 103:3389–3397. [PubMed: 20393066]

Brainard DH. The Psychophysics Toolbox. Spat Vis. 1997; 10:433–436. [PubMed: 9176952]

Desimone R, Albright TD, Gross CG, Bruce C. Stimulus-selective properties of inferior temporal neurons in the macaque. J Neurosci. 1984; 4:2051–2062. [PubMed: 6470767]

Desimone R, Ungerleider LG. Multiple visual areas in the caudal superior temporal sulcus of the macaque. J Comp Neurol. 1986; 248:164–189. [PubMed: 3722457]

DeYoe EA, Carman GJ, Bandettini P, Glickman S, Wieser J, Cox R, Miller D, Neitz J. Mapping striate and extrastriate visual areas in human cerebral cortex. Proc Natl Acad Sci U S A. 1996; 93:2382–2386. [PubMed: 8637882]

Dinstein I, Gardner JL, Jazayeri M, Heeger DJ. Executed and observed movements have different distributed representations in human aIPS. J Neurosci. 2008; 28:11231–11239. [PubMed: 18971465]

Dougherty RF, Ben-Shachar M, Bammer R, Brewer AA, Wandell BA. Functional organization of human occipital-callosal fiber tracts. Proc Natl Acad Sci U S A. 2005; 102:7350–7355. [PubMed: 15883384]

Downing PE, Jiang Y, Shuman M, Kanwisher N. A cortical area selective for visual processing of the human body. Science. 2001; 293:2470–2473. [PubMed: 11577239]

Downing PE, Wiggett AJ, Peelen MV. Functional magnetic resonance imaging investigation of overlapping lateral occipitotemporal activations using multi-voxel pattern analysis. J Neurosci. 2007; 27:226–233. [PubMed: 17202490]

Dumoulin SO, Bittar RG, Kabani NJ, Baker CL Jr, Le Goualher G, Bruce Pike G, Evans AC. A new anatomical landmark for reliable identification of human area V5/MT: a quantitative analysis of sulcal patterning. Cereb Cortex. 2000; 10:454–463. [PubMed: 10847595]

Dumoulin SO, Wandell BA. Population receptive field estimates in human visual cortex. Neuroimage. 2008; 39:647–660. [PubMed: 17977024]

Felleman DJ, Van Essen DC. Distributed hierarchical processing in the primate cerebral cortex. Cereb Cortex. 1991; 1:1–47. [PubMed: 1822724]

Filimon F, Nelson JD, Huang RS, Sereno MI. Multiple parietal reach regions in humans: cortical representations for visual and proprioceptive feedback during on-line reaching. J Neurosci. 2009; 29:2961–2971. [PubMed: 19261891]

Georgieva S, Peeters R, Kolster H, Todd JT, Orban GA. The processing of three-dimensional shape from disparity in the human brain. J Neurosci. 2009; 29:727–742. [PubMed: 19158299]

Glover GH. Simple analytic spiral K-space algorithm. Magn Reson Med. 1999; 42:412–415. [PubMed: 10440968]

Grill-Spector K, Kanwisher N. Visual recognition: as soon as you know it is there, you know what it is. Psychol Sci. 2005; 16:152–160. [PubMed: 15686582]

Grill-Spector K, Knouf N, Kanwisher N. The fusiform face area subserves face perception, not generic within-category identification. Nat Neurosci. 2004; 7:555–562. [PubMed: 15077112]

Grill-Spector K, Malach R. The human visual cortex. Annu Rev Neurosci. 2004; 27:649–677. [PubMed: 15217346]

Gross CG. Single neuron studies of inferior temporal cortex. Neuropsychologia. 2008; 46:841–852. [PubMed: 18155735]

Gross CG, Bender DB, Rocha-Miranda CE. Visual receptive fields of neurons in inferotemporal cortex of the monkey. Science. 1969; 166:1303–1306. [PubMed: 4982685]

Gross CG, Rocha-Miranda CE, Bender DB. Visual properties of neurons in inferotemporal cortex of the Macaque. J Neurophysiol. 1972; 35:96–111. [PubMed: 4621506]

Hansen KA, Kay KN, Gallant JL. Topographic organization in and near human visual area V4. J Neurosci. 2007; 27:11896–11911. [PubMed: 17978030]

Heider B, Karnik A, Ramalingam N, Siegel RM. Neural Representation During Visually Guided Reaching in Macaque Posterior Parietal Cortex. J Neurophysiol. 2010

Huk AC, Dougherty RF, Heeger DJ. Retinotopy and functional subdivision of human areas MT and MST. J Neurosci. 2002; 22:7195–7205. [PubMed: 12177214]

Jastorff J, Clavagnier S, Gergely G, Orban GA. Neural Mechanisms of Understanding Rational Actions: Middle Temporal Gyrus Activation by Contextual Violation. Cereb Cortex. 2010

Kaas JH. From mice to men: the evolution of the large, complex human brain. J Biosci. 2005; 30:155–165. [PubMed: 15886451]

Kaas JH, Morel A. Connections of visual areas of the upper temporal lobe of owl monkeys: the MT crescent and dorsal and ventral subdivisions of FST. J Neurosci. 1993; 13:534–546. [PubMed: 8381166]

Kanwisher N. Functional specificity in the human brain: a window into the functional architecture of the mind. Proc Natl Acad Sci U S A. 2010; 107:11163–11170. [PubMed: 20484679]

Kanwisher N, McDermott J, Chun MM. The fusiform face area: a module in human extrastriate cortex specialized for face perception. J Neurosci. 1997; 17:4302–4311. [PubMed: 9151747]

Kolster H, Peeters R, Orban GA. The retinotopic organization of the human middle temporal area MT/V5 and its cortical neighbors. J Neurosci. 2010; 30:9801–9820. [PubMed: 20660263]

Larsson J, Heeger DJ. Two retinotopic visual areas in human lateral occipital cortex. J Neurosci. 2006; 26:13128–13142. [PubMed: 17182764]

Levy I, Schluppeck D, Heeger DJ, Glimcher PW. Specificity of human cortical areas for reaches and saccades. J Neurosci. 2007; 27:4687–4696. [PubMed: 17460081]

May JG, Andersen RA. Different patterns of corticopontine projections from separate cortical fields within the inferior parietal lobule and dorsal prelunate gyrus of the macaque. Exp Brain Res. 1986; 63:265–278. [PubMed: 3530793]

Nestares O, Heeger DJ. Robust multiresolution alignment of MRI brain volumes. Magn Reson Med. 2000; 43:705–715. [PubMed: 10800036]

Op de Beeck HP, Haushofer J, Kanwisher NG. Interpreting fMRI data: maps, modules and dimensions. Nat Rev Neurosci. 2008; 9:123–135. [PubMed: 18200027]

Oram MW, Perrett DI. Integration of form and motion in the anterior superior temporal polysensory area (STPa) of the macaque monkey. J Neurophysiol. 1996; 76:109–129. [PubMed: 8836213]

Orban GA, Claeys K, Nelissen K, Smans R, Sunaert S, Todd JT, Wardak C, Durand JB, Vanduffel W. Mapping the parietal cortex of human and non-human primates. Neuropsychologia. 2006; 44:2647–2667. [PubMed: 16343560]

Orlov T, Makin TR, Zohary E. Topographic representation of the human body in the occipitotemporal cortex. Neuron. 2010; 68:586–600. [PubMed: 21040856]

Peelen MV, Downing PE. Selectivity for the human body in the fusiform gyrus. J Neurophysiol. 2005; 93:603–608. [PubMed: 15295012]

Peelen MV, Downing PE. The neural basis of visual body perception. Nat Rev Neurosci. 2007; 8:636–648. [PubMed: 17643089]

Peelen MV, Downing PE. Using multi-voxel pattern analysis of fMRI data to interpret overlapping functional activations. Trends Cogn Sci. 2007; 11:4–5. [PubMed: 17129747]

Peelen MV, Wiggett AJ, Downing PE. Patterns of fMRI activity dissociate overlapping functional brain areas that respond to biological motion. Neuron. 2006; 49:815–822. [PubMed: 16543130]

Pinsk MA, Arcaro M, Weiner KS, Kalkus JF, Inati SJ, Gross CG, Kastner S. Neural representations of faces and body parts in macaque and human cortex: a comparative FMRI study. J Neurophysiol. 2009; 101:2581–2600. [PubMed: 19225169]

Pinsk MA, DeSimone K, Moore T, Gross CG, Kastner S. Representations of faces and body parts in macaque temporal cortex: a functional MRI study. Proc Natl Acad Sci U S A. 2005; 102:6996–7001. [PubMed: 15860578]

Pitzalis S, Sereno MI, Committeri G, Fattori P, Galati G, Patria F, Galletti C. Human v6: the medial motion area. Cereb Cortex. 2010; 20:411–424. [PubMed: 19502476]

Sayres R, Grill-Spector K. Relating retinotopic and object-selective responses in human lateral occipital cortex. J Neurophysiol. 2008; 100:249–267. [PubMed: 18463186]

Schwarzlose RF, Baker CI, Kanwisher N. Separate face and body selectivity on the fusiform gyrus. J Neurosci. 2005; 25:11055–11059. [PubMed: 16306418]

Schwarzlose RF, Swisher JD, Dang S, Kanwisher N. The distribution of category and location information across object-selective regions in human visual cortex. Proc Natl Acad Sci U S A. 2008; 105:4447–4452. [PubMed: 18326624]

Sherbondy AJ, Dougherty RF, Ben-Shachar M, Napel S, Wandell BA. ConTrack: finding the most likely pathways between brain regions using diffusion tractography. J Vis. 2008; 8(15):11–16.

Spiridon M, Fischl B, Kanwisher N. Location and spatial profile of category-specific regions in human extrastriate cortex. Hum Brain Mapp. 2006; 27:77–89. [PubMed: 15966002]

Stepniewska I, Collins CE, Kaas JH. Reappraisal of DL/V4 boundaries based on connectivity patterns of dorsolateral visual cortex in macaques. Cereb Cortex. 2005; 15:809–822. [PubMed: 15459077]

Tootell RB, Hadjikhani N, Hall EK, Marrett S, Vanduffel W, Vaughan JT, Dale AM. The retinotopy of visual spatial attention. Neuron. 1998; 21:1409–1422. [PubMed: 9883733]

Tootell RB, Hamilton SL, Silverman MS. Topography of cytochrome oxidase activity in owl monkey cortex. J Neurosci. 1985; 5:2786–2800. [PubMed: 2995611]

Tootell RB, Reppas JB, Kwong KK, Malach R, Born RT, Brady TJ, Rosen BR, Belliveau JW. Functional analysis of human MT and related visual cortical areas using magnetic resonance imaging. J Neurosci. 1995; 15:3215–3230. [PubMed: 7722658]

Tootell RB, Taylor JB. Anatomical evidence for MT and additional cortical visual areas in humans. Cereb Cortex. 1995; 5:39–55. [PubMed: 7719129]

Tsao DY, Freiwald WA, Knutsen TA, Mandeville JB, Tootell RB. Faces and objects in macaque cerebral cortex. Nat Neurosci. 2003; 6:989–995. [PubMed: 12925854]

Walters NB, Egan GF, Kril JJ, Kean M, Waley P, Jenkinson M, Watson JD. In vivo identification of human cortical areas using high-resolution MRI: an approach to cerebral structure-function correlation. Proc Natl Acad Sci U S A. 2003; 100:2981–2986. [PubMed: 12601170]

Wandell BA, Chial S, Backus BT. Visualization and measurement of the cortical surface. J Cogn Neurosci. 2000; 12:739–752. [PubMed: 11054917]

Wandell BA, Dumoulin SO, Brewer AA. Visual field maps in human cortex. Neuron. 2007; 56:366–383. [PubMed: 17964252]

Watson JD, Myers R, Frackowiak RS, Hajnal JV, Woods RP, Mazziotta JC, Shipp S, Zeki S. Area V5 of the human brain: evidence from a combined study using positron emission tomography and magnetic resonance imaging. Cereb Cortex. 1993; 3:79–94. [PubMed: 8490322]

Weiner KS, Grill-Spector K. Sparsely-distributed organization of face and limb activations in human ventral temporal cortex. Neuroimage. 2010; 52:1559–1573. [PubMed: 20457261]

Weiner KS, Sayres R, Vinberg J, Grill-Spector K. fMRI-adaptation and category selectivity in human ventral temporal cortex: regional differences across time scales. J Neurophysiol. 2010; 103:3349–3365. [PubMed: 20375251]

Winawer J, Horiguchi H, Sayres RA, Amano K, Wandell BA. Mapping hV4 and ventral occipital cortex: the venous eclipse. J Vis. 2010:10. [PubMed: 20616143]

Worsley KJ, Poline JB, Friston KJ, Evans AC. Characterizing the response of PET and fMRI data using multivariate linear models. Neuroimage. 1997; 6:305–319. [PubMed: 9417973]

Zeki S. Thirty years of a very special visual area, Area V5. J Physiol. 2004; 557:1–2. [PubMed: 15034128]

Zeki S, Watson JD, Lueck CJ, Friston KJ, Kennard C, Frackowiak RS. A direct demonstration of functional specialization in human visual cortex. J Neurosci. 1991; 11:641–649. [PubMed: 2002358]

Research Highlights

1. Not one EBA: 3 limb-selective clusters in a crescent organization surrounding hMT+.
2. Each limb-selective cluster has a distinct anatomical location.
3. LO and TO visual field maps verify parcellation of LOTC limb-selective activations.
4. Differential position and body part selectivity across LOTC limb-selective activations.
5. New multi-factor criteria for parcellating high-level visual cortex using fMRI.

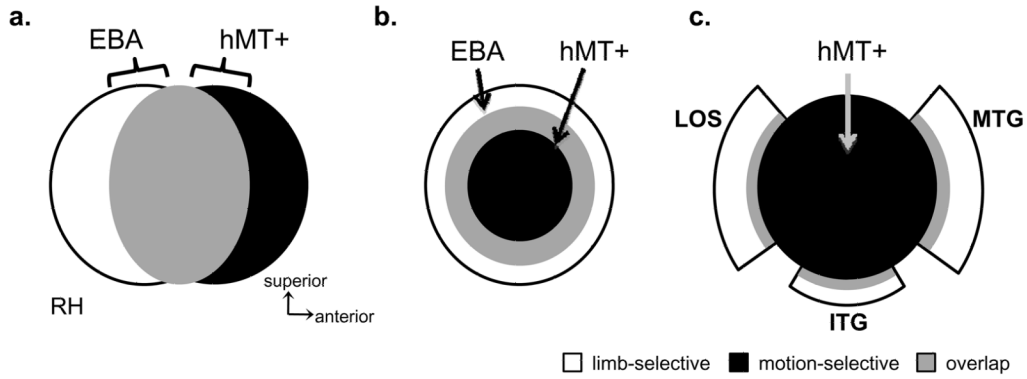


**Figure 1. Three potential spatial relationships between limb-selective activations and hMT+**

(a) Highly overlapping EBA and hMT+, where the EBA is largely posterior to hMT+ and the two activations overlap on the posterior portion of the inferotemporal sulcus (based on Peelen and Downing, 2006; Peelen and Downing, 2007). (b) Highly overlapping EBA and hMT+ where the EBA is a ring surrounding hMT+, which is located as a central, non-overlapping region within the posterior inferotemporal sulcus (based on Spiridon et al., 2006). (c) Three separate limb-selective components in distinct anatomical locations surrounding hMT+ in a crescent organization (based on the anatomical distinction between MT and MT crescent in humans; Tootell and Taylor, 1995). *Acronyms*: LOS: lateral occipital sulcus; ITG: inferotemporal gyrus; MTG: middle temporal gyrus.

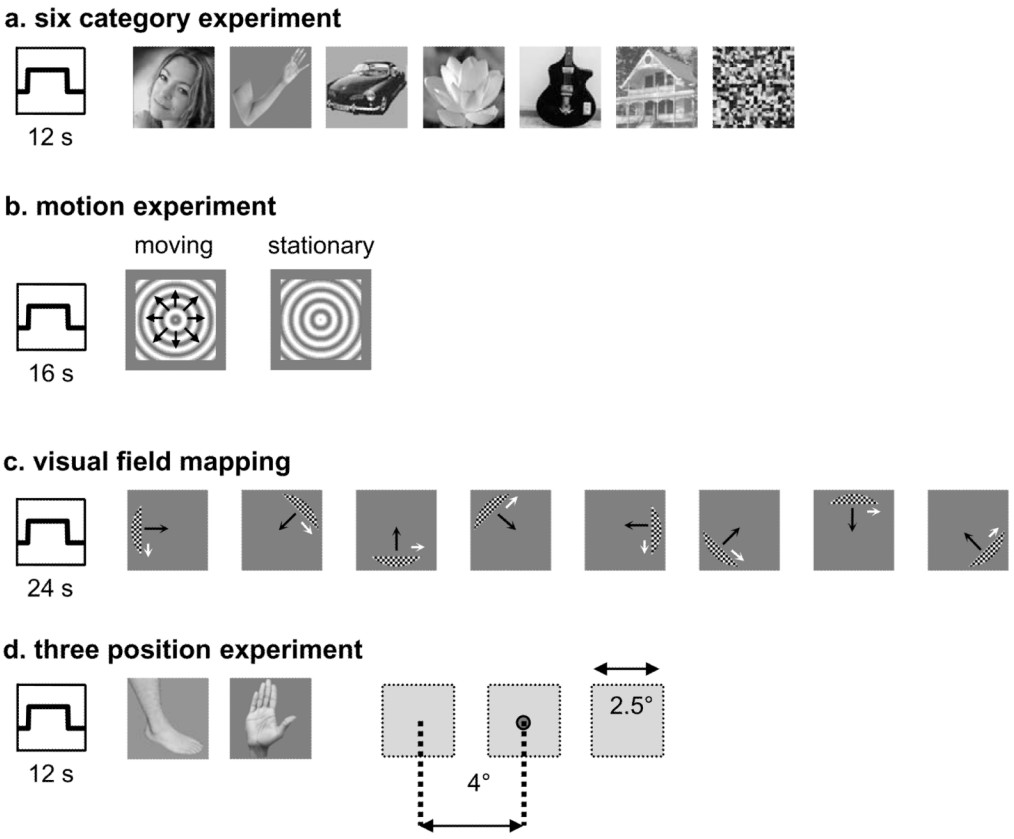


**Figure 2. Experimental designs**

(a) *Six category experiment*. Sessions 1 (1.5 × 1.5 × 3mm voxels) and 2 (1.5 mm isotropic voxels) contained blocks lasting 12-s where each image was presented for 750-ms followed by a 250-ms blank. Blocks included gray-level images of faces, limbs, flowers, cars, guitars, houses, scrambled images, or a mean luminance screen with a fixation cross. Subjects were required to fixate and to detect by button press when an image repeated (1-back task). (b) *Motion experiment*. Sessions 1 (1.5 × 1.5 × 3 mm) and 2 (1.5 mm isotropic) contained blocks lasting 16-s, which alternated between low contrast expanding and contracting concentric gratings and identical stationary gratings. Subjects fixated while viewing the stimuli. (c) *Visual field mapping.* A moving bar aperture revealed a portion of the underlying checkerboard stimulus. The bar moved smoothly across visual space in eight different directions (4 cardinal directions plus 4 diagonals), completing one sweep every 24-s. The bar aperture disappeared four times during the scan, leaving a mean-luminance screen for 12-s. Subjects were required to fixate and to perform a color discrimination task on the fixation dot during each run. Black arrows indicate the direction in which the aperture moved, while white arrows indicate the direction in which the checkerboard pattern moved within the aperture (arrows are used for illustration purposes and did not appear in the actual experiment). (d) *Three position experiment*. Images of limbs (both upper and lower) were presented 4° to the right or to the left of fixation, as well as at fixation (e.g. foveal presentation). Images subtended 2.5° of visual angle at each position. In each 12-s block, different images were shown at a specific position.

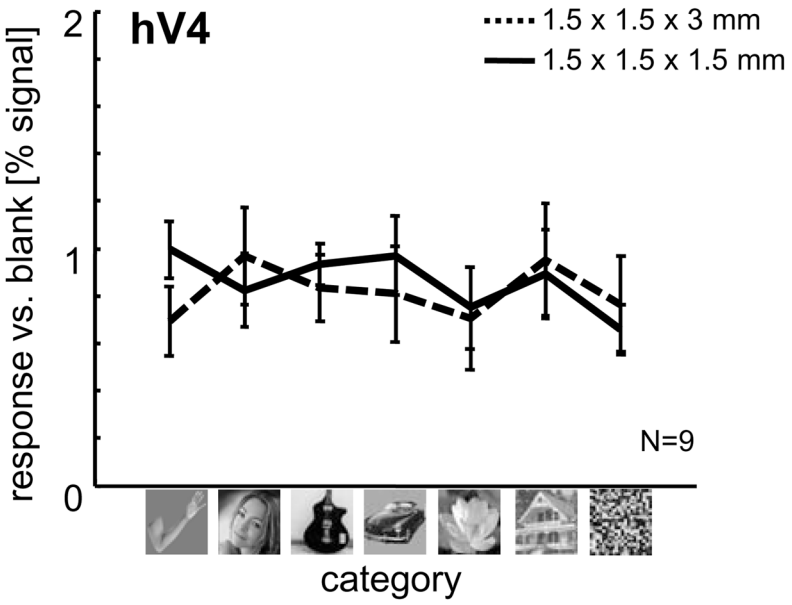


**Figure 3. hV4 illustrates reproducible measurements across sessions, but no category-selective responses**

After defining hV4 from the independent visual field mapping experiments, time courses from the six category localizer were extracted from Session 1 (1.5 × 1.5 × 3mm voxels; dotted black line) and Session 2 (1.5mm isotropic; solid black line). Results are threefold: (1) BOLD responses to images from different categories are not greater than scrambled versions of these exemplars, (2) BOLD responses to images from a particular category were not greater than responses to images from other categories, indicating that the observed limb-selective responses reported throughout the manuscript are not due to low-level visual features across image categories, and (3) measurements are reproducible across sessions.

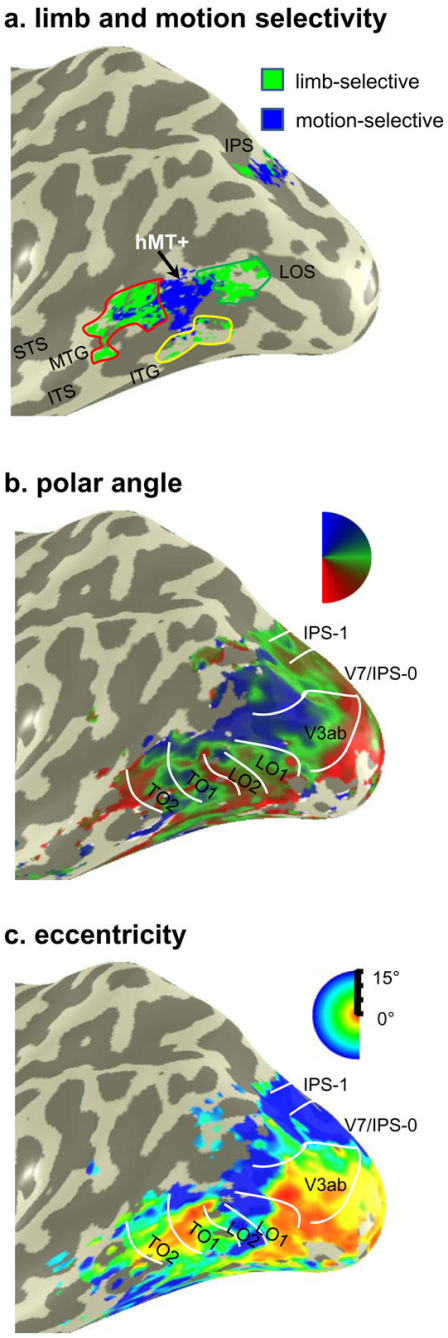


**Figure 4. Limb-selectivity, motion-selectivity, and visual field maps in human LOTC**

(a) Limb-selective activations defined as limbs > all other categories ($t > 3$, voxel level; green) and motion-selective activations defined as moving > static concentric gratings ($t > 3$, voxel level; blue) on the inflated cortical left hemisphere of subject S2. Colored outlines illustrate the delineation of three separate limb-selective activations surrounding hMT+ based on anatomical location: MTG (red), ITG (yellow), and LOS/MOG (green). (b) Polar angle representations in the same example subject. Polar angle representation and boundaries of visual field maps LO-1/2, TO-1/2, V3ab, V7/IPS-0, and IPS-1. (c) Eccentricity representations in the same example subject. *Acronyms*: ITS: inferotemporal

sulcus; STS: superior temporal sulcus; ITG: inferotemporal gyrus; MTG: middle temporal gyrus; LOS: lateral occipital sulcus; IPS: intraparietal sulcus.

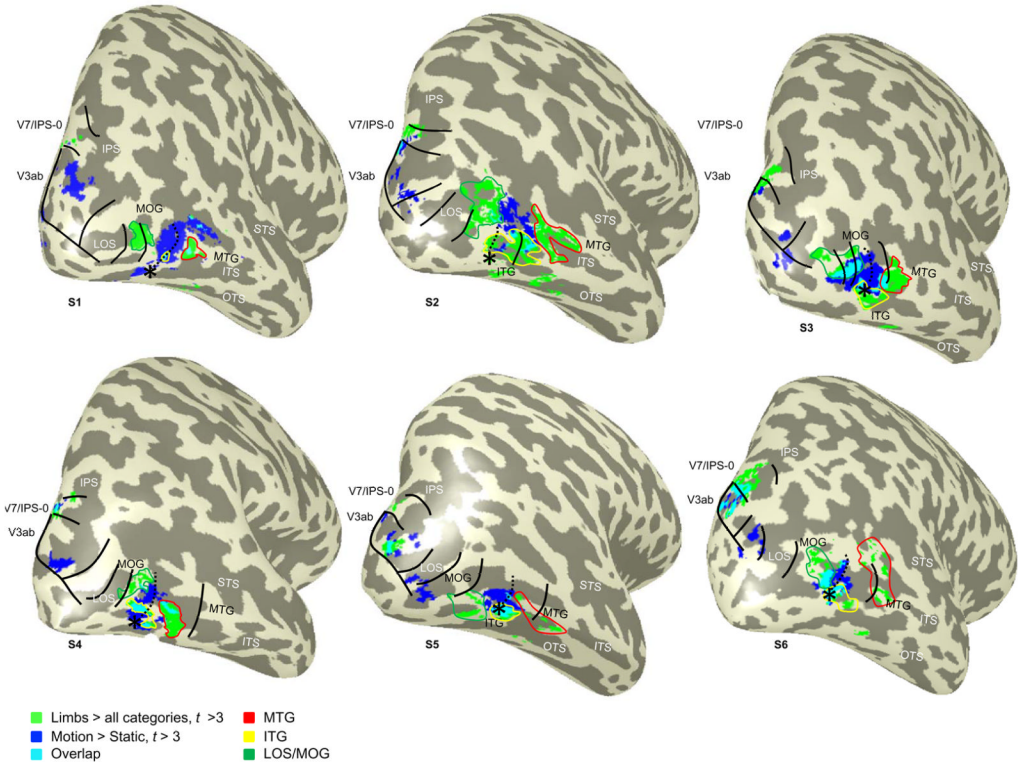


**Figure 5. Three limb-selective activations surround hMT+ and overlap with separate visual field maps**

Six example subjects with limb-selective (limbs > all other categories, $t > 3$, voxel level; green) and motion-selective (moving > static concentric gratings, $t > 3$, voxel level; blue) activations, as well as their overlap (cyan), from the six category and motion experiments in session one overlaid on the inflated right hemisphere. Black outlines indicate hemifield reversals of visual field maps, where the dotted line represents the TO-1/TO-2 boundary, and the asterisk illustrates the TO fovea. The limb-selective LOS/MOG largely falls on the lower field representation shared between LO-2 and TO-1, while the ITG activation falls on the parafovea of the TO cluster, and the MTG activation falls on the lower field representation of TO-2 and extends outside known visual field maps. As in Figure 3, colored outlines illustrate the delineation of the three separate limb-selective activations surrounding hMT+ based on anatomy: MTG (red), ITG (yellow), and LOS/MOG (green). Relevant gyri are labeled in black and relevant sulci labeled in white. *Acronyms*: ITS: inferotemporal sulcus; STS: superior temporal sulcus; ITG: inferotemporal gyrus; MTG: middle temporal gyrus; LOS: lateral occipital sulcus; IPS: intraparietal sulcus; OTS: occipitotemporal sulcus; MOG: middle occipital gyrus.

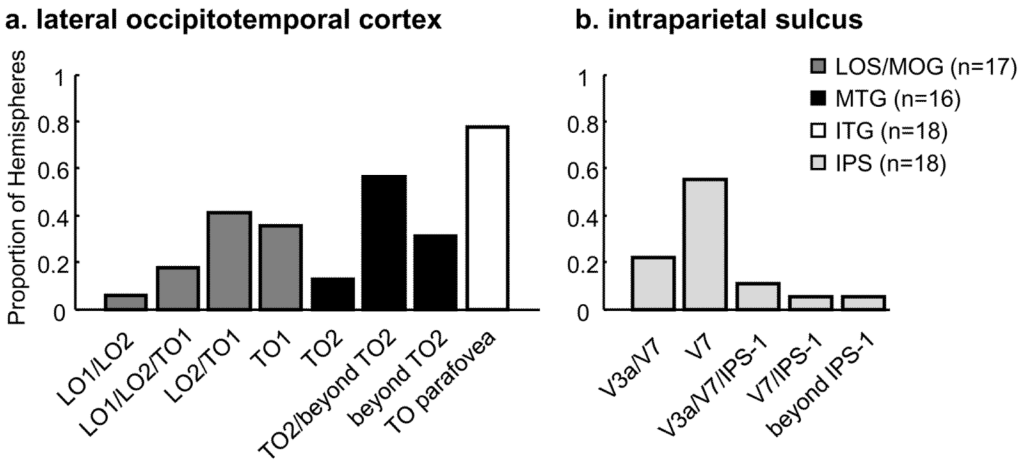


**Figure 6. Histograms summarizing the overlap between limb-selective activations and visual field maps**

The proportion of hemispheres that overlap with either a specific visual field map or a combination of visual field maps for each of the limb-selective activations in (a) lateral occipitotemporal cortex (LOTC) and (b) the intraparietal sulcus (IPS). (a) In LOTC, there is not a one-to-one mapping between visual field map and location of the limb-selective activation, but rather each limb-selective activation typically falls across a combination of visual field maps. The LOS/MOG overlaps with LO-2/TO-1 and the MTG overlaps with TO-2 and extends outside known visual field maps, with neither activation overlapping the upper vertical meridian shared between TO-1 and TO-2. The ITG activation overlaps with the TO parafovea. (b) Limb-selective IPS largely overlaps with V7.

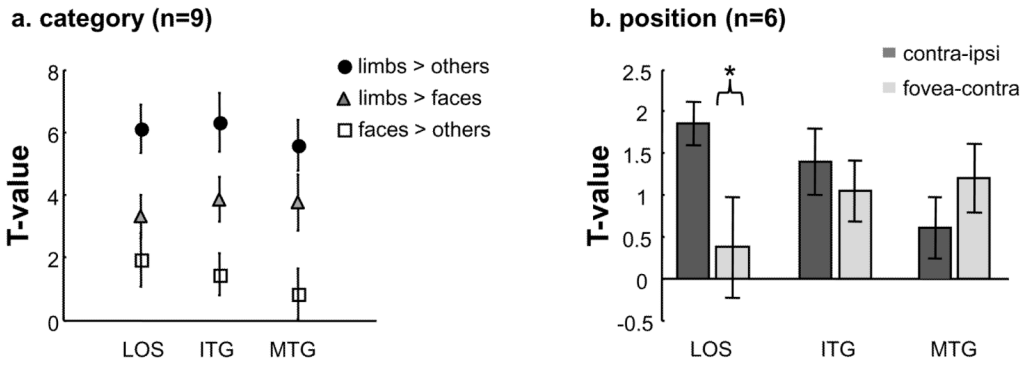


**Figure 7. Consistent limb selectivity and different position sensitivity among LOTC limb-selective activations**

(a) Using the ROIs defined from the six category experiment in session one, timecourses from session two were extracted and *t*-values were calculated three different ways: limbs > others (flowers, cars, guitars, and houses), limbs > faces, and faces > others. Not only is there consistent limb selectivity relative to the four other categories (circles) and faces (triangles) across the three LOTC regions, but there is also decreasing face selectivity (squares) where the limb-selective MTG does not illustrate significantly positive face selectivity. Error bars indicate SEMs. (b) Using the ROIs defined from the six category experiment in session one, timecourses from the three position experiment were extracted and *t*-values were calculated for contralateral (contralateral vs. ipsilateral) and foveal (foveal vs. contralateral) biases in the LOS/MOG, ITG, and MTG limb-selective activations. The limb-selective LOS/MOG illustrates a significantly greater contralateral bias than foveal bias, while the ITG and MTG do not. *Asterisk:* contralateral bias is significantly stronger than foveal bias, $p < .05$. Error bars indicate SEMs.

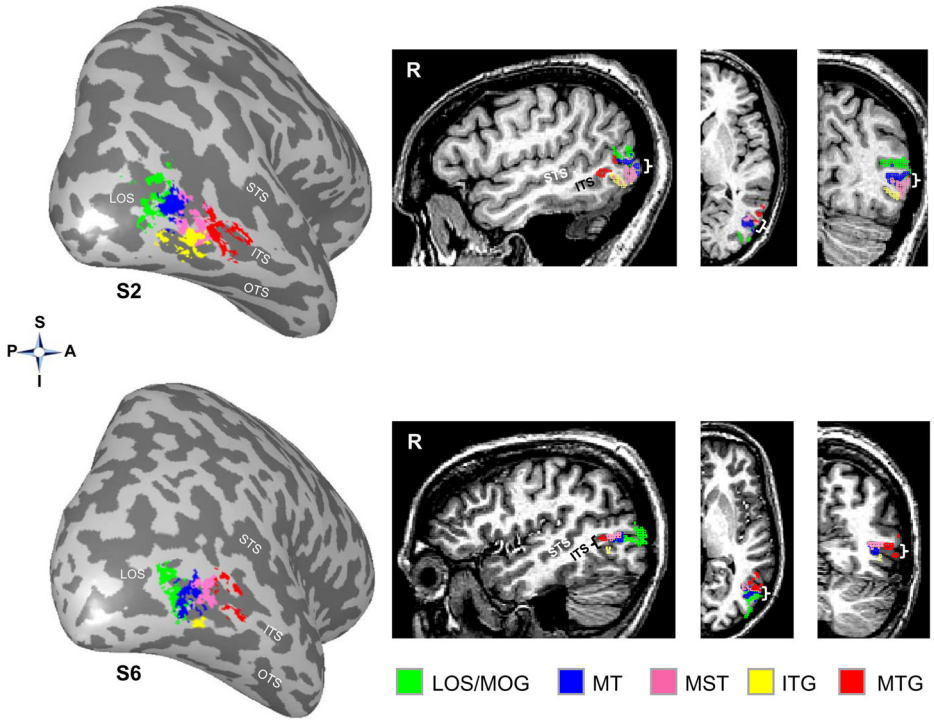


**Figure 8. Limb-selective activations relative to MT and MST**

Limb-selective activations LOS/MOG (green), ITG (yellow), and MTG (red) in the right hemisphere of two example subjects. *Left:* 3D surface reconstruction; *Right:* sagittal, axial, and coronal volume views. Note that hMT+ can be divided into two functional subcomponents, MT and MST, that are both located between the LOTC limb-selective activations. Brackets indicate the location of the ITS on the volume slices. *Acronyms:* S: Superior; I: Inferior; P: Posterior; A: Anterior.

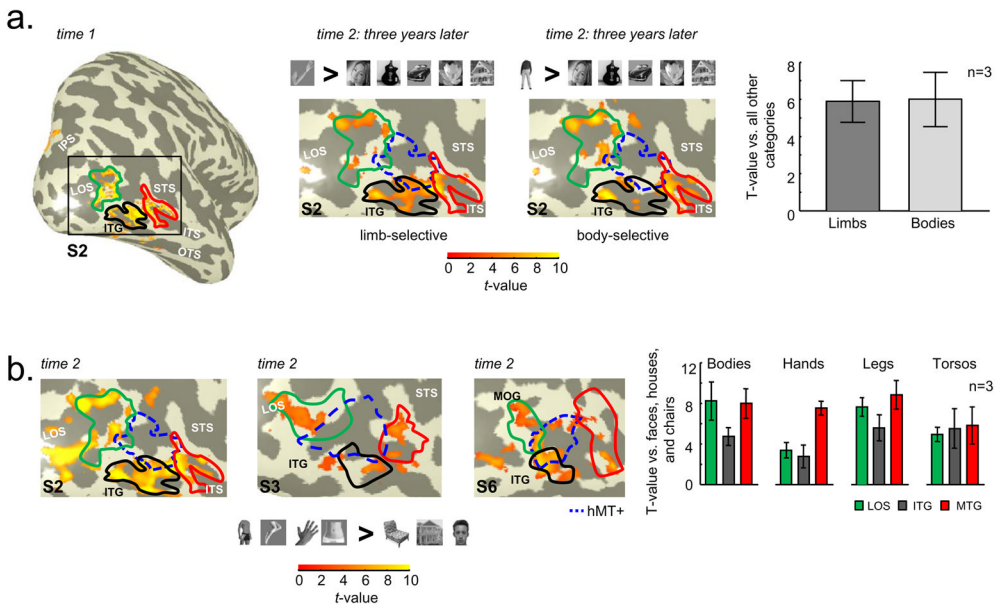


**Figure 9. Crescent organization surrounding hMT+ is consistent over three years and across stimuli used to define selective LOTC voxels**

(a) Far left panel: Lateral view of the inflated right hemisphere of subject S2 illustrating the statistical contrast of limbs > all categories ($t > 3$, voxel level) at time 1, which is the same data as in Figure 5. Middle two panels: Zoomed view of LOTC indicated by the black rectangle. *Left:* Same contrast of limbs > other categories ($t > 3$, voxel level) in subject S2 three years later. *Right:* Headless Bodies > other categories ($t > 3$, voxel level). Headless body images were the same stimuli used in Downing et al., 2007. hMT+ indicated in blue outline and limb-selective LOS/MOG, ITG, and MTG defined from time 1 outlined in green, black, and red, respectively. *Far right:* Within the union of LOTC limb-selective voxels independently defined at time 1, the average *t*-value of these voxels illustrates no difference between limb and body selectivity (stimulus > other categories) at time 2 three years later. (b) *Left three panels*: Zoomed view of the right LOTC in three example subjects for the contrast of headless bodies, torsos, legs, hands > faces, houses, and chairs ($t > 3$, voxel level) at time 2. Headless body, torso, and leg images were the same stimuli used in Orlov et al., 2010. Chair images were the same stimuli used in Downing et al., 2007. Limb-selective LOS/MOG, ITG, and MTG defined from time 1 outlined in green, black, and red, respectively. hMT+ is indicated in blue outline. *Far right:* Using the ROIs from time 1, the *t*-values for each body part stimulus were extracted relative to faces, houses, and chairs. Each ROI shows a different profile of response, which both replicates Orlov et al., 2010 and Bracci et al., 2010, as well as extends these results by illustrating that these body part-selective voxels radiate around hMT+ and largely fall outside areas MT and MST.

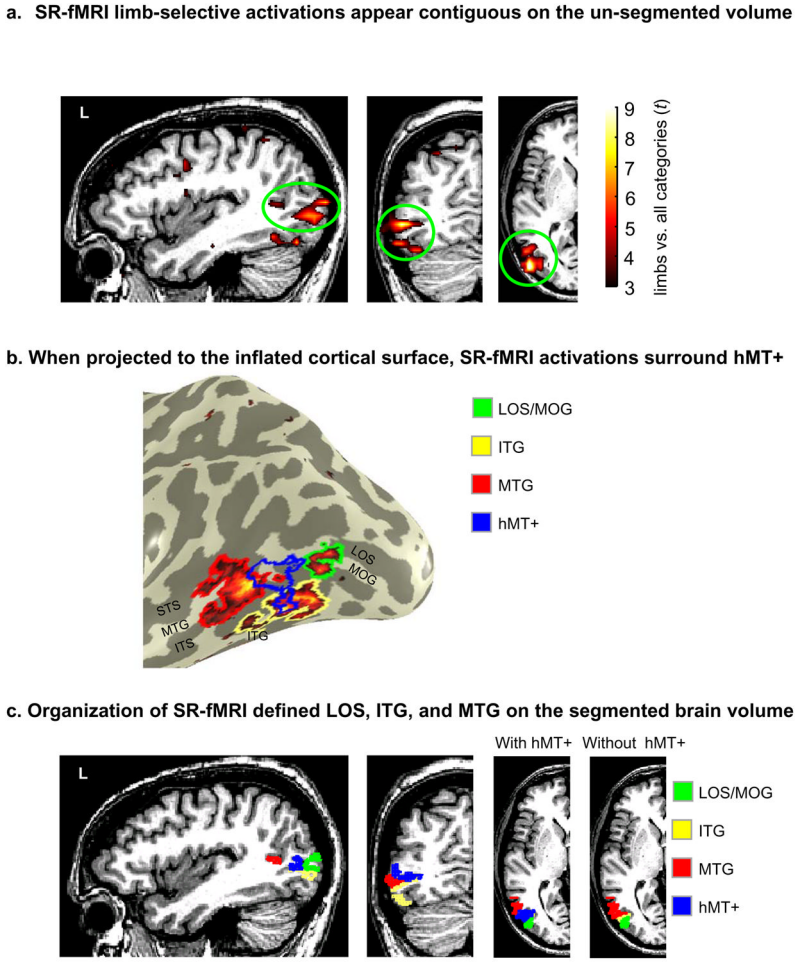


**Figure 10. A guide for defining separate LOTC limb-selective activations on the volume with standard resolution fMRI**

(a) Statistical contrast of limbs > all categories ($t > 3$, voxel level) from the six category experiment in subject S2 using voxels eight times as large as our original acquisition (3.75 × 3.75 × 4mm compared to 1.5 × 1.5 × 3mm illustrated in Figure 3a). The green circle indicates what researchers would define as the EBA based on what appears as a contiguous activation using an un-segmented volume visualization. (b) When projecting the same activation map along with hMT+ onto the corresponding inflated cortical surface, the three separate limb-selective activations are clearly illustrated as we find with high-resolution fMRI. (c) When restricting activations to the gray matter and adding the location of hMT+, the separation of the LOS/MOG and MTG limb-selective activations becomes clearer even in the volume view (see rightmost panel). Using sagittal and axial slices (left and right, respectively), hMT+ is a sufficient division boundary to separate the LOS/MOG from the MTG.

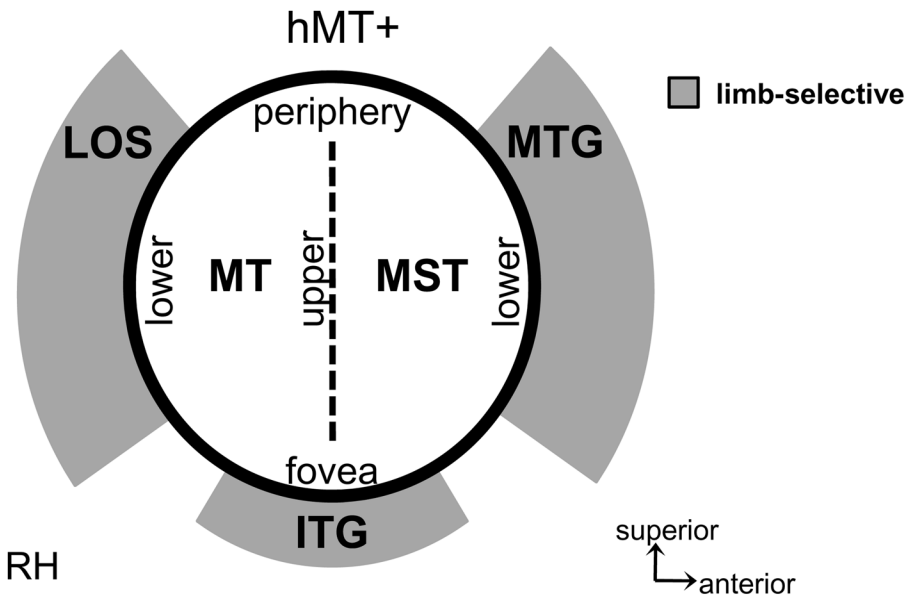


**Figure 11. Summary of the spatial relationship among limb- and motion-selective activations relative to visual field maps in human LOTC**

There are three limb-selective activations located on separate anatomical locations surrounding the perimeter of the human MT+ complex. The limb-selective LOS/MOG overlaps with the lower vertical meridian shared between LO-2 and TO-1, where TO-1 also corresponds to area MT of the hMT+ complex. The limb-selective MTG overlaps with the lower vertical meridian of TO-2, where TO-2 also corresponds to area MST of the hMT+ complex. The ITG overlaps the inferior portions of TO-1 and TO-2 most consistently on the parafoveal representation of the TO cluster. No limb-selective voxels are found within the upper vertical meridian shared between MT (TO-1) and MST (TO-2).

## Table 1

**Reproducibility and relationship between multivoxel patterns of response in LOTC**

Values indicate the correlations between multivoxel patterns (MVP) for motion, limbs, faces, and cars within an anatomical LOTC ROI across the same experiments and subjects acquired in different sessions about five months apart (Session 1: 1.5. × 1.5 × 3 mm voxels; Session 2: 1.5 mm isotropic voxels). Italicized entries illustrate values significantly greater than 0 ($p < .04$), while bold entries illustrate values significantly less than 0 ($p < 10^{-4}$). Values in parentheses signify the SEM across subjects (N = 6).

| | **Motion** | **Limbs** | **Faces** | **Cars** |
|---|---|---|---|---|
| Motion | *.29 (±.05)* | **-.13 (±.02)** | **-.22 (±.04)** | -.09(±.06) |
| Limbs | | *.25(±.06)* | -.02 (.04) | -.08 (±.05) |
| Faces | | | *.32 (±.05)* | *.07(±.03)* |
| Cars | | | | *.23(±.06)* |